CONJUGATED POLYMERS AND POLYELECTROLYTES IN SOLAR PHOTOCONVERSION

DE-FG02-03ER15484

Final Technical Report covering the period from March 2010 to March 2014

PI: Kirk S. Schanze[1]
Co-PIs: Valeria D. Kleiman[1] and John R. Reynolds[1,2]

[1] Department of Chemistry, University of Florida, Gainesville, FL 32611-7200

[2] Current Address: School of Chemistry and Biochemistry, School of Materials Science and Engineering, Georgia Institute of Technology, Atlanta, GA 30332-0400

kschanze@chem.ufl.edu, reynolds@chemistry.gatech.edu, kleiman@chem.ufl.edu

1. Project Summary and Objectives

Conjugated polymers feature unique properties due to the delocalized electronic structure of the π-conjugated backbone.[1,2] These properties include (semi)conductivity, strong visible light absorption and light emission, both of which are important to application of conjugated polymers in light harvesting and energy conversion. Because the electronic and optical properties are determined by the molecular structure of the monomers and the polymer repeat unit structure, synthetic organic and polymer chemistry can be used to tailor and control the properties.[3] Considerable effort from organic, polymer, physical and materials chemists has focused on the development of a broad spectrum of conjugated polymers, with much current interest focused on integrating these structures into polymer-based photovoltaics.[4-6]

Conjugated polyelectrolytes (CPEs) combine a π-conjugated backbone with polyelectrolyte character imparted by substitution of the arylene repeat units with ionic solubilizing groups (e.g., $-SO_3^-$, $-CO_2^-$, $-NMe_3^+$).[7-9] The conjugated backbone imparts a CPE with its electronic and optical properties, while the polyion structure renders the polymers soluble in and processable from water and polar organic solvents. Prototypical CPE structures are illustrated below in Figure 1 along with a photograph illustrating the ability to control the optical properties with the repeat unit structure.

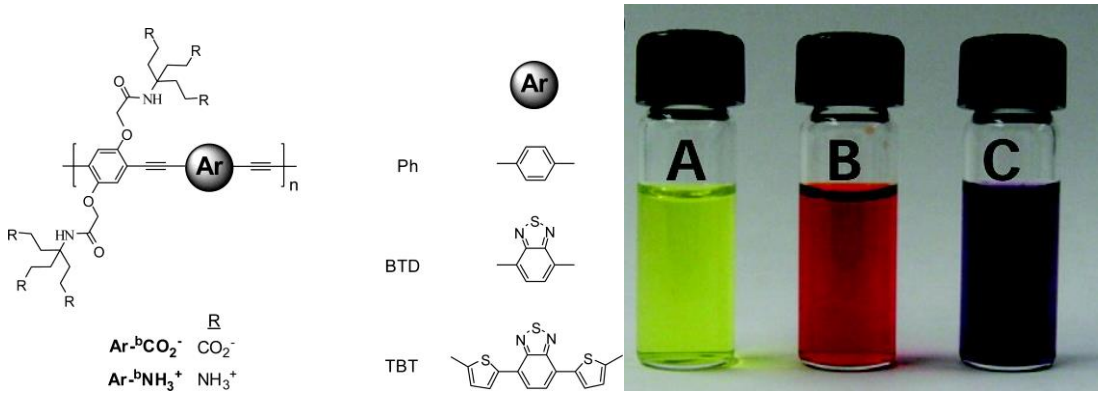

Figure 1. Chemical structures of a series of anionic and cationic arylene ethynylene based conjugated polyelectrolytes. Photo at right is of aqueous solutions of the CPEs with anionic side groups (Ar-$^bCO_2^-$) with Ph (A), BTD (B) and TBT (C) repeat units. For more information please see ref. [10].

This DOE-supported program is investigating the fundamental properties of conjugated polyelectrolytes, with emphasis placed on studies of excited state energy transport, self-assembly into CPE-based films and colloids, and exciton transport and charge injection in CPE films constructed atop wide bandgap semiconductors. In the most recent grant period we have also extended efforts to examine the properties of low-bandgap donor-acceptor conjugated polyelectrolytes that feature strong visible light absorption and the ability to adsorb to metal-oxide interfaces. In order to address the program objectives, a team of three PIs with complementary expertise is working together: Reynolds (monomer and polymer synthesis, electronic and optical properties of polymeric materials, photoconversion in solar cells), Schanze (polymer, dendrimer and oligomer synthesis, photophysics, and photoconversion) and Kleiman (ultrafast spectroscopy of molecular and macromolecular systems). Over the past several years this program has had the following objectives:

1. Design, synthesis and characterization of structurally-well defined conjugated polyelectrolyte structures, including conjugated polyelectrolyte dendrimers (CPDs) and conjugated polyelectrolyte oligomers (CPOs).
2. Investigation of the photophysical properties of CPD and CPO structures, including the study of ultrafast energy transport dynamics in these structurally-well defined conjugated polyelectrolyte structures.
3. Development of fluorescence correlation spectroscopy (FCS) as a sensitive probe for aggregation in conjugated polyelectrolyte systems.
4. Design, synthesis and photophysical characterization of novel electron donor-acceptor ion-containing conjugated oligomer systems.
5. Study of the physical and photoelectrochemical properties of CPE films adsorbed on crystalline and nanostructured TiO_2 interfaces.

Publications resulting from the investigation that have issued between 2010 and 2012 are listed on the following page,[10-24] and complete copies of these manuscripts are attached at the end of the proposal. In the following sections, key results from the work carried out to date are highlighted, with some emphasis placed on results that set the stage for the work that is described in the proposal.

Publications Resulting from DOE Support, 2011 – 2014

1. Lee, S. H.; Kömürlü, S.; Zhao, X. Y.; Jiang, H.; Moriena, G.; Kleiman, V. D.; Schanze, K. S., Water-Soluble Conjugated Polyelectrolytes with Branched Polyionic Side Chains, *Macromolecules* **2011**, *44*, 4742-4751, 10.1021/ma200574d.
2. Fang, Z.; Eshbaugh, A. A.; Schanze, K. S., Low-Bandgap Donor-Acceptor Conjugated Polymer Sensitizers for Dye-Sensitized Solar Cells, *J. Am. Chem. Soc.* **2011**, *133*, 3063-3069, 10.1021/ja109926k.
3. Bricaud, Q.; Fabre, R. M.; Brookins, R. N.; Schanze, K. S.; Reynolds, J. R., Energy Transfer between Conjugated Polyelectrolytes in Layer-by-Layer Assembled Films, *Langmuir* **2011**, *27*, 5021-5028, 10.1021/la105113k.
4. Kömürlü, S.; Lee, S. H.; McCarley, T.; Schanze, K. S.; Kleiman, V. D., Energy Transfer in Extended Thienylene-Phenylene-Ethynylene Dendrimers, *J. Phys. Chem. B* **2011**, *115*, 15214-15220, 10.1021/jp2089802.
5. Sambur, J. B.; Averill, C. M.; Bradley, C.; Schuttlefield, J.; Lee, S. H.; Reynods, J. R.; Schanze, K. S.; Parkinson, B. A., Interfacial Morphology and Photoelectrochemistry of Conjugated Polyelectrolytes Adsorbed on Single Crystal TiO_2, *Langmuir* **2011**, *27*, 11906-11916, 10.1021/la201837v.
6. Xie, D. P.; Parthasarathy, A.; Schanze, K. S., Aggregation-Induced Amplified Quenching in Conjugated Polyelectrolytes with Interrupted Conjugation, *Langmuir* **2011**, *27*, 11732-11736, 10.1021/la202122p.
7. Feng, F.; Lee, S. H.; Schanze, K. S., "Light Switch" Effect Upon Binding of Ru-dppz to Water-Soluble Conjugated Polyelectrolyte Dendrimers, *J. Phys. Chem. Lett.* **2012**, *3*, 1707-1710, 10.1021/jz3005738.
8. Patel, D. G.; Feng, F. D.; Ohnishi, Y. Y.; Abboud, K. A.; Hirata, S.; Schanze, K. S.; Reynolds, J. R., It Takes More Than an Imine: The Role of the Central Atom on the Electron-Accepting Ability of Benzotriazole and Benzothiadiazole Oligomers, *J. Am. Chem. Soc.* **2012**, *134*, 2599-2612, 10.1021/ja207978v.
9. Wu, D.; Feng, F.; Xie, D.; Chen, Y.; Tan, W.; Schanze, K. S., Helical Conjugated Polyelectrolyte Aggregation Induced by Biotin-Avidin Interaction, *J. Phys. Chem. Lett.* **2012**, *3*, 1711-1715, 10.1021/jz300452t.
10. Feng, F.; Lee, S. H.; Cho, S. W.; Komurlu, S.; McCarley, T.; Roitberg, A.; Kleiman, V. D.; Schanze, K. S., Conjugated Polyelectrolyte Dendrimers: Aggregation, Photophysics and Amplified Quenching, *Langmuir* **2012**, *28*, 16679-16691, 10.1021/la303641m.
11. Vella, J. H.; Parthasarathy, A.; Schanze, K. S., Triplet Sensitization in an Anionic Poly(phenyleneethynylene) Conjugated Polyelectrolyte by Cationic Iridium Complexes, J. Phys. Chem. A **2013**, *117*, 7818-7822, 10.1021/jp405577z.
12. Feng, F.; Yang, J.; Xie, D.; McCarley, T. D.; Schanze, K. S., Remarkable Photophysics and Amplified Quenching of Conjugated Polyelectrolyte Oligomers, *J. Phys. Chem. Lett.* **2013**, *4*, 1410-1414, 10.1021/jz400421g.
13. Yang, J.; Wu, D.; Xie, D.; Feng, F.; Schanze, K. S., Ion-Induced Aggregation of Conjugated Polyelectrolytes Studied by Fluorescence Correlation Spectroscopy, *J. Phys.Chem. B* **2013**, *117*, 16314-16324, 10.1021/jp408370e.

14. Zhu, X.; Nepomnyashchii, A. B.; Roitberg, A. E.; Parkinson, B. A.; Schanze, K. S., Photosensitization of Single-Crystal ZnO by a Conjugated Polyelectrolyte Designed to Avoid Aggregation, *J. Phys. Chem. Lett.* **2013**, *4*, 3216-3220.
15. Koenen, J. M.; Zhu, X. Z.; Pan, Z. X.; Feng, F. D.; Yang, J.; Schanze, K. S., Enhanced Fluorescence Properties of Poly(phenylene ethynylene)-Conjugated Polyelectrolytes Designed to Avoid Aggregation, *ACS Macro Lett.* **2014**, *3*, 405-409, 10.1021/mz500067k.
16. Richard, C. A.; Pan, Z.; Hsu, H.-Y.; Cekli, S.; Schanze, K. S.; Reynolds, J. R., Effect of Isomerism and Chain Length on Electronic Structure, Photophysics, and Sensitizer Efficiency in Quadrupolar (Donor)(2)-Acceptor Systems for Application in Dye-Sensitized Solar Cells, *ACS Appl. Mater. Interfaces* **2014**, *6*, 5221-5227.
17. Richard, C. A.; Pan, Z.; Parthasarathy, A.; Arroyave, F. A.; Estrada, L. A.; Schanze, K. S.; Reynolds, J. R., Quadrupolar (donor)(2)acceptor-acid chromophores for dye-sensitized solar cells: influence of the core acceptor, *J. Mater. Chem. A* **2014**, *2*, 9866-9874.

2. Conjugated Polyelectrolytes. Dendrimers, Oligomers and Polymers

2.1. Overview of CPE Structures.

Much of our work in the area of CPEs has focused on the study of the structure and dynamics of their excited states. We have been particularly interested in understanding the "amplified quenching" effect that arises when the fluorescent excited state of a CPE is quenched by an oppositely charged quencher ion.[25-29] In the most recent grant cycle our studies have focused on structurally well-defined conjugated polyelectrolytes, including conjugated polyelectrolyte dendrimers (CPDs) and conjugated polyelectrolyte oligomers (CPOs). This work has the goal of understanding the dynamics of exciton transport and amplified quenching in the absence of complicating features such as polydispersity in chain length and polymer aggregation in solution.

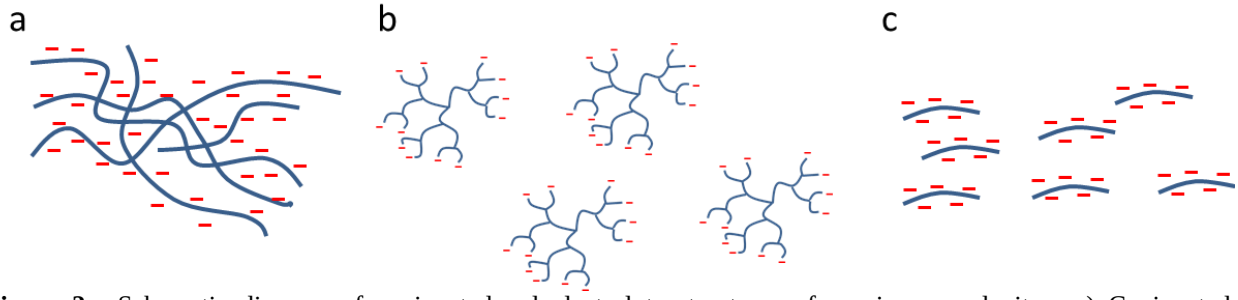

Figure 2. Schematic diagram of conjugated polyelectrolyte structures of varying complexity. a) Conjugated polyelectrolyte (CPE) aggregate; b) Conjugated polyelectrolyte dendrimers (CPD); c) mono-disperse conjugated polyelectrolyte oligomers (CPO).

In this work we have accomplished the complete synthesis and photophysical characterization of three families of conjugated polyelectrolyte dendrimers (CPD). Each of the CPDs is characterized by having a skeleton consisting of a fully conjugated arylene ethynylene network. At the terminus of each dendrimer branch is appended a tri-carboxylate unit which affords the structures with a highly polar, ionic periphery. As seen in more detail below, each of the first, second and third generation dendrimers features a net ionic charge of (-9), (-18) and (-36), respectively. The three families of CPD structures differ in the composition of the arylene units (phenylene vs. thienylene) and extent of conjugation within the CPD core. The difference in conjugation leads to a difference in the HOMO-LUMO gap, and consequently the photophysical properties of the CPDs.

A second, more focused line of recent work has led to the synthesis and photophysical characterization of a set of three conjugated polyelectrolyte oligomers (CPOs). This series features a 1,4-phenylene ethynylene conjugated backbone; and oligomers containing five, seven and nine repeats have been constructed. Each of the phenylene units in the CPOs contains a pair of -(CH_2COO^-) side-groups giving the CPOs net ionic charge of (-8), (-12) and (-16) for the pentamer, heptamer and nonamer, respectively.

In the following sections, we outline the details of the CPE, CPD and CPO structures that have been the focus of the recent work. In addition, we summarize the most significant findings of the photophysical studies.

2.2. Conjugated Polyelectrolyte Dendrimers: Structures and Synthesis

During the past 2 years, we have accomplished the synthesis of the three families of conjugated polyelectrolyte dendrimers shown below in Scheme 1.[19,22] Each of the sets of CPDs features a fully conjugated phenylene ethynylene (PE) backbone that emanates from a three-fold symmetric phenylene unit core. The CPDs are surrounded on the periphery by a branched tricarboxylate functionality, which was protected as a *tert*-butyl ester during the synthesis; the ester groups were removed at the final synthesis stage unmasking the ionic CPD forms. (The acronyms shown in Scheme 1 and used throughout the report distinguish between the ester precursors and the ionic forms as follows: ***PG*-n** refers to the ester protected dendrimer of generation "n", whereas ***G*-n** refers to the ionic dendrimer of generation "n".) Each set of CPDs was prepared in three generations (G-1, G-2 and G-3). The three families of CPDs differ in the core chromophore unit. In particular, series **PG-n** and **G-n** feature a conjugated backbone consisting entirely of meta-linked PE units. Series **Ph-PG-n** and **Ph-G-n** feature a three ring PE chromophore in the core, surrounded by a periphery consisting of meta-linked PE segments. Finally, in series **Th-PG-n** and **Th-G-n** the dendrimer core features a 2,5-thienylene linker inserted between the core phenylene unit and the first phenylene unit of the dendrimer periphery.

All of the dendrimers were synthesized by an iterative convergent-divergent synthesis strategy, with the primary reaction used being the Pd-catalyzed Sonogashira coupling between a terminal acetylene unit and an aryl halide (Ar-C≡C-H + Ar-X, where X = Br or I).[19,22,30] The number of steps required for the synthesis increased with generation number, with the third generations requiring ~15 individual steps. Most of the reactions proceeded in relatively high yield. However, the final coupling reactions used to assemble the second and third generation dendrimers were hindered by steric effects and the high molecular weight of the components, and yields < 20% were typical for the final coupling reactions. The final dendrimers were fully characterized for the ester protected forms (**PG-n**) using NMR and MALDI-TOF mass spectrometry. The ionic forms of the dendrimers were prepared by acid- or base-catalyzed hydrolysis of the ester protecting groups, with the final materials isolated as Na^+ salts.

While the detailed structure of the three families of dendrimers is distinct, they share the common feature of a planar, three-fold symmetric core unit. The influence of this structural aspect on the three-dimensional structure of the dendrimers was carefully explored using molecular dynamics simulations for the **Ph-PG-n** and **Ph-G-n** family. These simulations reveal that the ester dendrimers **Ph-PG-n** have a flat core, and the main structural difference between the different generations lies in the orientations of the peripheral branches. The peripheral ester substituents of **Ph-PG-1** are positioned far away from each other, whereas **Ph-PG-2** and **Ph-PG-3** possess crowded peripheral ester substituents which appear at times to come into close proximity, even when they are attached to adjacent dendrimer branches (see Figure 3a,b for the structure of **Ph-PG-3**). Visualization of the dynamics reveals that the disubstituted phenylene rings rapidly rotate around their long axis, whereas the trisubstituted rings undergo

Scheme 1

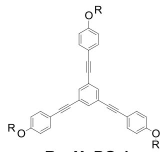

R = X: PG-1
R = Y: G-1

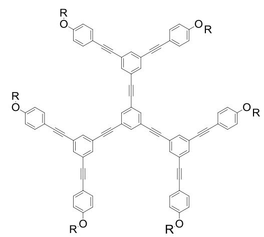

R = X: PG-2
R = Y: G-2

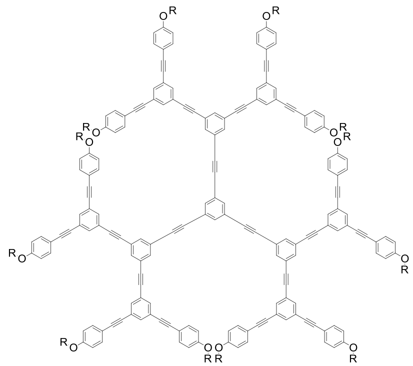

R = X: PG-3
R = Y: G-3

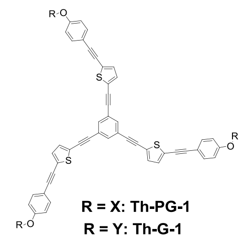

R = X: Th-PG-1
R = Y: Th-G-1

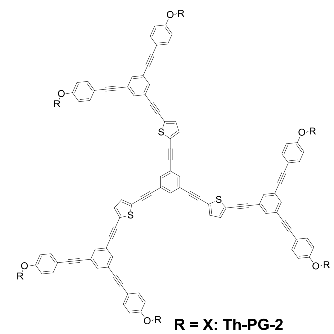

R = X: Th-PG-2
R = Y: Th-G-2

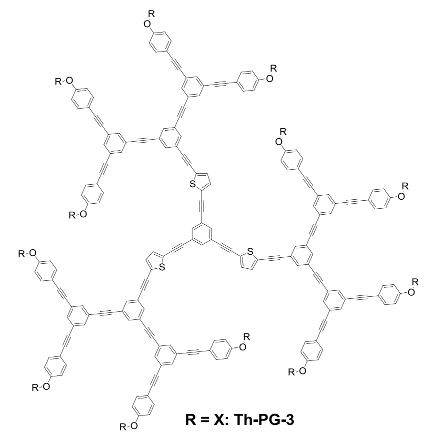

R = X: Th-PG-3
R = Y: Th-G-3

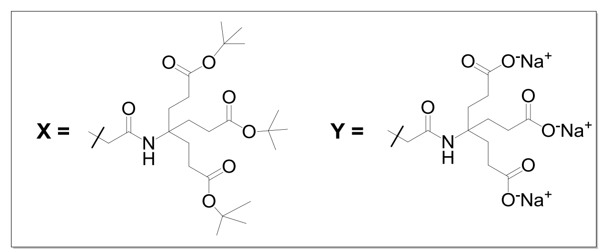

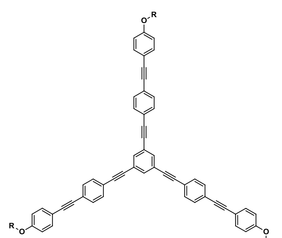

R = X: Ph-PG-1
R = Y: Ph-G-1

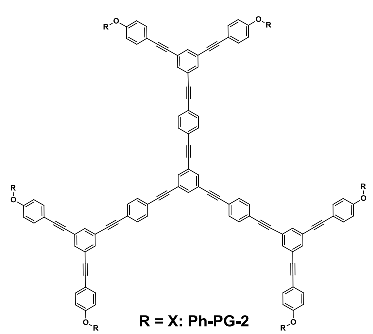

R = X: Ph-PG-2
R = Y: Ph-G-2

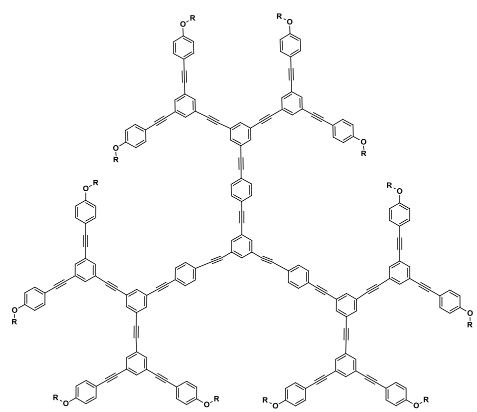

R = X: Ph-PG-3
R = Y: Ph-G-3

comparatively slower torsions. Because of the rotation of the phenylene units, the dendrimer branches are not always parallel to the plane of the core, resulting in a lowered overall planarity of the dendrimer structure (increasing with generation number). The results show that **Ph-PG-1** is relatively "flat" (95% of the conformations are less than 1 nm thick), whereas **Ph-PG-2** and **Ph-PG-3** are relatively less so, existing in conformations that are overall oblate in shape rather than spherical.

Simulations were also performed on the ionic dendrimers, **Ph-G-n**, in water solution. Overall the results are generally similar to those seen for the ester forms, but with a few important distinctions. First, **Ph-G-1** in water adopts a relatively flat conformation in analogy to **Ph-PG-1** in THF. The second and third generation CPDs also have relatively flat cores; however, electrostatic repulsion between the anionic carboxylate units in the dendrimer perhiphery leads to significant population of out-of-plane conformations arising from rotation of the trisubstituted phenylene rings. The significant result is that the conformations of **Ph-G-2** and **Ph-G-3** are more three-dimensional than those of corresponding ester-type dendrimers in THF (see Figures 3 c,d). Overall, we anticipate that due to their relatively more oblate structures, and the surrounding high negative charge density, **Ph-G-2** and **Ph-G-3** will be more stable in solution as molecularly dissolved CPDs. By contrast, as noted above, due to its relatively flat overall structure **Ph-G-1** is more likely to undergo self-assembly (due to hydrophobic interactions) to form supramolecular "pancake stack" assemblies. This is borne out by the photophysical results, see below.

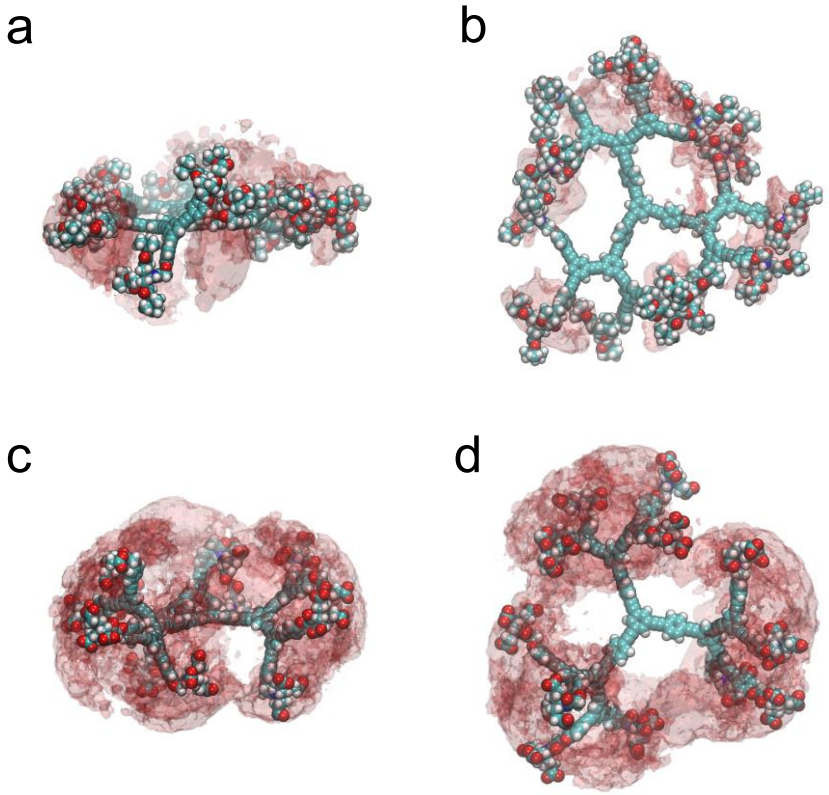

Figure 3. Oxygen occupancy contour images of a-b) **Ph-PG-3** (ester form) in THF, and c-d) **Ph-G-3** (ionic form) in water. The contours were obtained by plotting the position of the periperhy oxygens from a molecular dynamics trajectory. The contours illustrate the effective area sampled by the oxygen atoms during the trajectory.

2.3. Conjugated Polyelectrolyte Dendrimers: Photophysics and Amplified Quenching

Comprehensive photophysical investigations were carried out on of all of the CPDs shown in Scheme 1 and this work is described in a series of papers that are submitted or in the final stages of preparation.[19,22,30] In this progress report we provide an overview of this work, focusing on the most significant findings relevant to the overall objectives of the DOE program. The interested reader is directed to the manuscripts attached to the report for additional detail. Study of the ultrafast dynamics of excitations in the dendrimer systems are described below in section 3.

Below in Figure 4 we show the absorption and fluorescence spectra of two of the dendrimer series, **Ph-PG-n/Ph-G-n** and **Th-PG-n/Th-G-n**. The ester precursors (***PG*** series) are studied in THF solution, while the ionic forms (***G*** series) are studied in methanol and aqueous solutions. All of the dendrimers exhibit intense absorption in the near-UV region arising from the phenylene ethynylene conjugated backbone. However, the details of the absorption differ for the different series because of the different core chromophores. First, in each series the absorption of the first generation is characterized by a band in the near-UV region (350-400 nm). The higher generation dendrimers (G-2 and G-3) exhibit the same near-UV feature; but in addition, there is a significant increase in absorption at $\lambda \sim 300$ nm. This shorter wavelength band arises from the periphery of the dendrimers which contain chromophores with shorter conjugation length (interrupted by the meta-linkages). Interestingly, comparison of the absorption of the Ph and Th dendrimer series reveals that the latter show a well-resolved absorption band which is at longer wavelength (see arrows in Figure 4). This absorption is due to the core unit which consists of the phenylene-CC-2,5-thienylene-CC-phenylene chromophore.

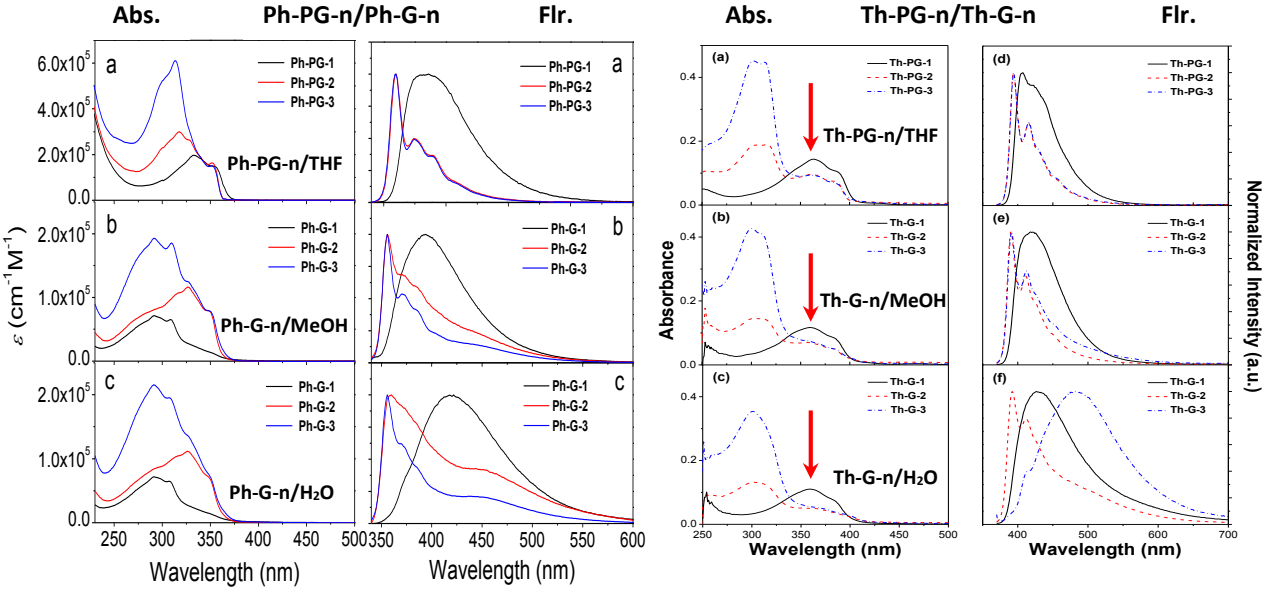

Figure 4. Absorption (left plots-Abs.) and fluorescence (right plots-Flr.) of **Ph-PG-n/Ph-G-n** and **Th-PG-n/Th-G-n** dendrimers in THF, MeOH and aqueous solution. Individual plots are labeled in the figure. Arrows in the absorption plots for Th-PG-n/Th-G-n indicate the position of the long-wavelength band for the thienylene core chromophore.

The Ph dendrimers also exhibit a long wavelength shoulder absorption that arises due to the core chromophore, phenylene-CC-1,4-phenylene-CC-phenylene. The long wavelength band is red-shifted for the Th series, due to the fact that incorporation of the 2,5-thienylene unit into the core chromophore decreases the HOMO-LUMO gap, presumably by raising the HOMO level.

There are interesting changes in the absorption spectra in the ionic CPDs, both in methanol and in aqueous solutions. In general the absorption spectra exhibit blue-shifts; this is especially evident in the absorption of the first generation CPDs, **Ph-G-1** and **Th-G-1**. We are confident that the blue shift for the G-1 CPDs arises due to H-aggregates formed by "card stack" aggregation (see below in Section 3.3 for more detail). However, the origin of the blue shifts for the G-2 and G-3 CPDs is less clear. We hypothesize that there may be some interdendrimer aggregation (formation of dimers or multimers); but in addition, it is possible that some of the aggregate-chromophore interactions could arise within individual dendrimer units due to collapse of the CPDs due to solvophobic interactions.

Careful inspection of the fluorescence spectra for the Ph-PG-n and Th-PG-n series in THF solutions reveals that the emission emanates exclusively from the core chromophore. This is evident by the fact that the 0-0 fluorescence band red-shifts nearly 40 nm going from the Ph to the Th dendrimers. The fluorescence is independent of excitation wavelength, which indicates that intradendrimer energy transfer is rapid. Fluorescence upconversion studies confirm the rapid energy transfer dynamics, and show that the transfer rates decrease slightly with increasing generation number (see Section 3.4 below). Evidence for inter-chromophore interactions is quite evident in the fluorescence spectra of the ionic CPDs in methanol and aqueous solution. The evidence consists of spectral broadening and an increase in the fluorescence decay lifetimes on the red-side of the fluorescence bands (see Figure 4, fluorescence of Ph-G-n series in water, bottom panel of second column from left).

A number of investigations have explored amplified fluorescence quenching of conjugated polyelectrolytes by oppositely charged quencher ions. For example, anionic poly(phenylene vinylene)s and poly(phenylene ethynylene)s are quenched with very high efficiency by positively charged quencher ions, in particular pyridinium salts such as N,N'-dimethylviologen (MV^{2+}).[27,28,31,32] An objective of this study was to explore whether conjugated polyelectrolyte dendrimers exhibit the amplified quenching effect. In particular, we were especially interested in exploring quenching under conditions where the CPDs are not aggregated.

Generally similar results were found in the quenching studies of all three sets of CPDs; here we show details of the quenching of the **Ph-G-n** series. Quenching studies were carried out in water with the concentration of each CPD set at 1 μM, and the Stern-Volmer (SV) plots (I_0/I - 1 vs. $[MV^{2+}]$) are shown in Figure 5. First, it is evident that the overall quenching efficiency increases sharply with the CPD generation number. Stern-Volmer constants (K_{SV}) determined from the initial slopes of the quenching plots are 1.8×10^5 M^{-1} (**Ph-G-1**), 1.3×10^6 M^{-1} (**Ph-G-2**) and 4.7×10^6 M^{-1} (**Ph-G-3**). Aside from the difference in overall efficiency, the SV plots for the **Ph-G-n** series differ with generation number. Specifically, for **Ph-G-1** and **Ph-G-2** the plots exhibit downward curvature (e.g., less efficient quenching at higher $[MV^{2+}]$), while that of **Ph-G-3** features slightly upward curvature (which is more typical of a system exhibiting amplified quenching). The downward curvature in the SV plots for the **Ph-G-1** and **Ph-G-2** is believed to

arise due to the presence of multimer aggregates in the CPD solutions. In essence, there are likely regions with the CPD assemblies where the MV^{2+} quencher is not able to come within close proximity to the fluorescent core chromophores.

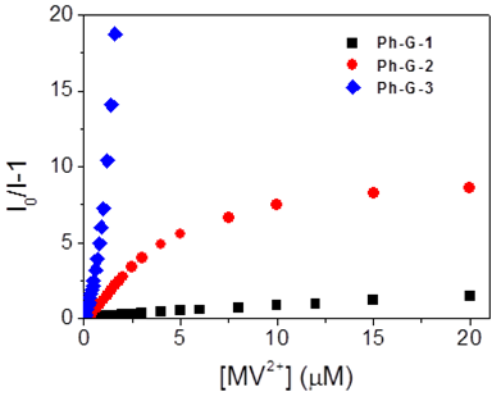

Figure 5. Stern-Volmer plot of **Ph-G-n**s (n = 1, 2 and 3, c = 1.0 μM) in water as a function of MV^{2+} concentration.

The quenching efficiency is most remarkable in **Ph-G-3**, with >90% quenching observed at $[MV^{2+}]$ = 1.0 μM MV^{2+} and 98% quenching at 2.5 μM. Importantly, the 90% quenching efficiency is seen at 1:1 **Ph-G-3**:MV^{2+} stoichiometry - indicating that on average a single viologen is able to quench the emission of an entire **Ph-G-3** macromolecule. In order to examine the dynamics of the MV^{2+} quenching process, the fluorescence lifetime of **Ph-G-3** was monitored as a function of $[MV^{2+}]$. This experiment finds that the lifetime is nearly unchanged over a range of added quencher where the emission intensity is reduced 5-fold. Thus, the quenching process is very fast on the timescale of the TCSPC system (resolution ~100 ps), indicating that "static quenching" dominates. Overall, this quenching behavior of the **Ph-G-3**/MV^{2+} system is very similar to that observed when anionic conjugated polyelectrolytes are quenched by MV^{2+}.[31-33]

2.4. Conjugated Polyelectrolyte Oligomers

Towards the objective of studying photophysics and amplified quenching in conjugated polyelectrolytes in the absence of complications arising from chain length polydispersity and aggregation, we designed and synthesized the series of oligomers shown below in Scheme 2. Specifically, three oligomers were prepared, each of which features a phenylene ethynylene backbone that is functionalized with side groups that contain carboxylic acid ester or sodium carboxylate solubilizing groups. The oligomers feature 5, 7 or 9 phenylene ethynylene (PE) repeat units, and they are named **PEn**(**Na**) where n refers to the number of PE repeats and the Na label indicates the sodium carboxylate ionic form. These oligomers were synthesized by an iterative-convergent methodology in which Sonogashira coupling reactions played an important role in many of the key steps. The oligomers' synthesis and purification was carried out with the carboxyl groups protected as dodecyl (C_{12}) and t-butyl ester groups (for the terminal phenylene units), and in the final synthesis steps the ester groups were removed by hydrolysis affording the

Scheme 2

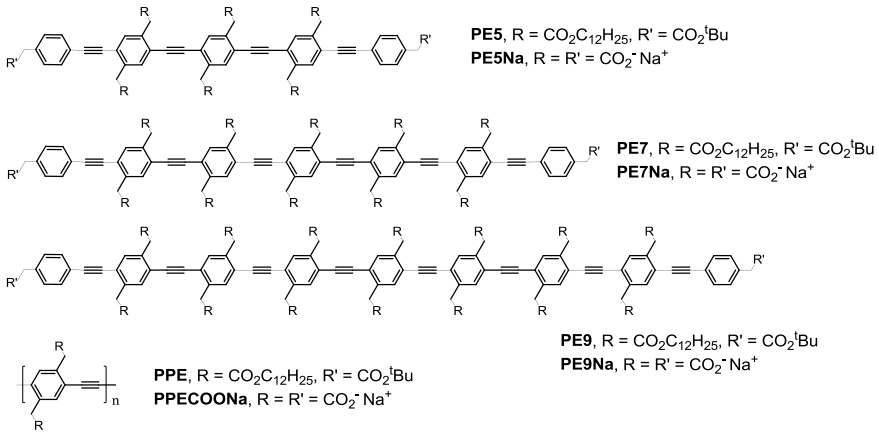

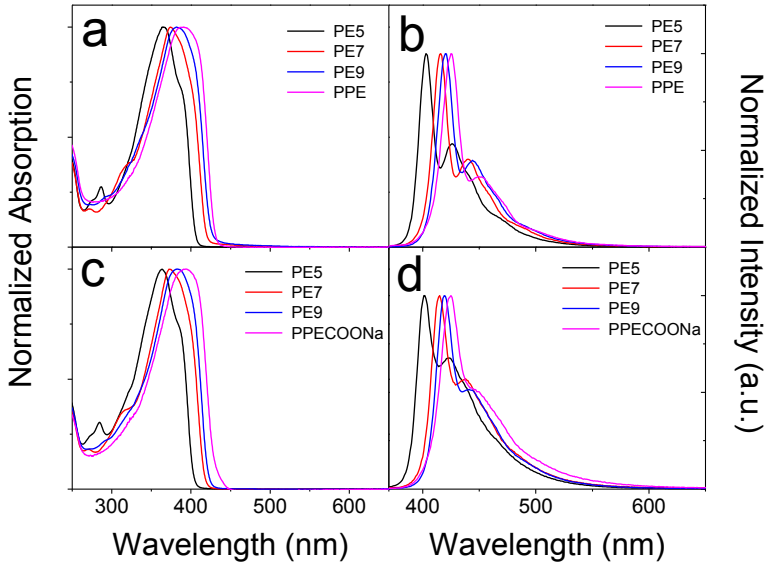

Figure 6. Normalized absorption spectra of a) **PEn** in $CHCl_3$ and b) **PEnNa** in H_2O. Normalized fluorescence spectra of c) **PEn**s in $CHCl_3$ and d) **PEnNa**s in H_2O, λ_{ex} = 360 nm.

Table 1. Photophysical properties of PEn and PEnNa oligomers

	$CHCl_3$				H_2O			
	PE5	**PE7**	**PE9**	**PPE**	**PE5Na**	**PE7Na**	**PE9Na**	**PPECOONa**
λ_{max},nm	364	374	382	391	364	374	383	391
λ_{em},nm	403	416	420	425	402	415	419	425
Φ_F	0.78[a]	1.00[a]	0.92[a]	0.52[a]	0.69[a]	0.73[a]	0.94[a]	0.42[a]
τ, ns	0.50	0.46	0.41	0.33	0.69	0.58	0.51	0.42
k_r, s^{-1}	1.6×10^9	2.2×10^9	2.2×10^9	1.6×10^9	1.0×10^9	1.3×10^9	1.8×10^9	1.0×10^9
k_{nr}, s^{-1}	4.4×10^8	0	2.0×10^8	1.5×10^9	4.5×10^8	4.7×10^8	1.2×10^8	1.4×10^9

[a]Quinine sulfate in 0.1 M H_2SO_4 is used as actinometer, Φ_F=0.545.

ionic forms, **PEnNa**. We also preserved samples of the organic soluble ester protected forms to allow comparison of the photophysical properties of the esters in organic solvents with the ionic forms in aqueous solution.

The oligomers display remarkable photophysical properties, both in the ester protected and ionic forms. Most importantly, as seen above in Figure 6 and Table 1, the absorption and fluorescence of the oligomers are essentially the same for the ester forms in $CHCl_3$ and the ionic forms in water (**PEn** and **PEnNa** series, respectively). The similarity extends to the fluorescence quantum yields, which are very high in every case, approaching unity in some instances (e.g., **PE7Na** and **PE9Na**)! This finding is very significant, as in all of our previous studies we have found that the fluorescence of ionic CPEs in water is substantially different from that of the corresponding organic soluble ester derivatives. In particular, typically the fluorescence of the ionic form CPEs in water is red-shifted, spectrally broadened, and much weaker ($\phi < 0.1$) compared to that of the organic soluble ester form.[34] The difference in optical properties for the CPEs in water has been attributed to the effects of aggregation, where interchain contacts create "excimer like" traps for the single excitons. The significance of the result on the **PEnNa** oligomers is that the results strongly suggest that these compounds do not aggregate in aqueous solution, rather they exist in a molecularly dissolved state.

We have also examined the Stern-Volmer (SV) fluorescence quenching behavior of the anionic **PEnNa** oligomers when they are exposed to low concentrations of cationic quencher ions, Figure 7. These quenching experiments used MV^{2+}, which quenches by electron transfer, and the cationic cyanine dye DOC, which quenches by singlet-singlet (Förster) energy transfer. There are several significant features that emerge from the quenching studies. First, the quenching constants (K_{SV}) are very large for all of the oligomer/quencher combinations, with values in excess of 10^6 M^{-1} in every case for MV^{2+} quencher, and in excess of 10^7 M^{-1} for the longer oligomers with DOC quencher. The observed K_{SV} values are comparable to those observed for quenching of high-molecular weight conjugated polyelectrolytes by viologens or cyanine dyes,[25,32,35] where the large quenching response has been attributed to the "amplified quenching effect". This significant result clearly indicates that amplified quenching is active in the oligomers (despite their modest chain length), and if we can clearly understand their solution properties (see below), we may gain significant insight into the mechanism of the amplified quenching phenomenon.

Another important result of the SV quenching studies emerges from consideration of the stoichiometry for the quenching experiments with DOC. In particular, for this DOC quenching of **PE9Na** we find 90% quenching is achieved at an oligomer:dye concentration ratio of ~3:1. This means that a single dye can effectively quench the fluorescence of *three* oligomer molecules. The result must be interpreted as indicating that on average a single DOC quencher is within the Förster radius (~50 Å) of at least three oligomer molecules. If the oligomers are randomly distributed in solution at a concentration of 1 μM the average separation distance is ~75 nm. Given this result, we are forced to conclude that the oligomers cannot be randomly distributed in the solution (i.e., molecularly dissolved); rather, they must exist as weakly interacting multimer or aggregates which bind to the dye molecules allowing a single dye to interact with and quench multiple oligomers.

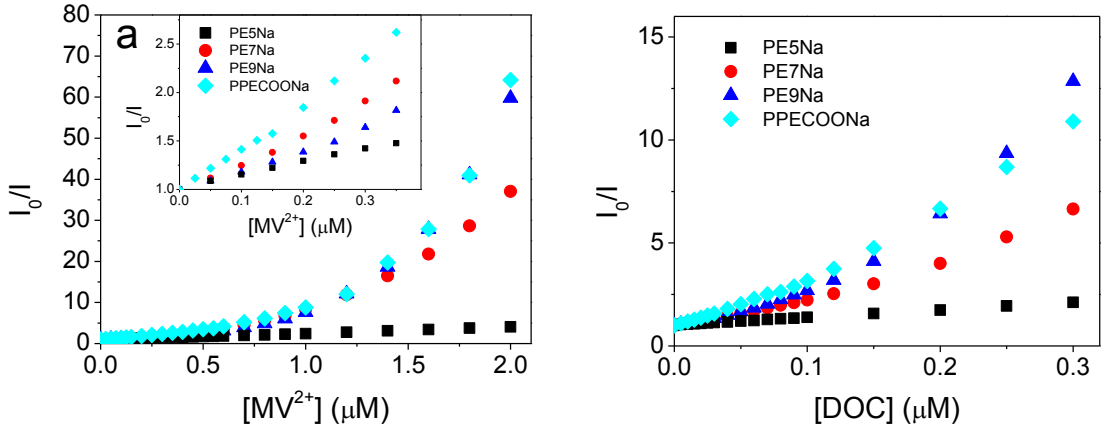

Figure 7. Stern-Volmer quenching of **PEnNa** oligomers by MV^{2+} (left) and cyanine dye DOC (right). Oligomer concentration is 1 μM throughout.

3. Time Resolved Studies of Exciton Dynamics in Conjugated Polyelectrolytes

3.1. Overview

Conjugated dendrimers are antennae/chromophore systems with molecularly well-defined architectures that can contain a rich arrangement of chromophore units. As the size of the dendrimer increases, there are conformational changes from planar to globular structures. For the conjugated dendrimers at the center of this work (Scheme 1), the HOMO-LUMO gap or lowest-lying electronic energy can be modulated by changing the chemical composition of the core structure. Additionally, a vectorial energy gradient can be anticipated due to the difference in gap for the core and peripheral units. Addition of ionizable end-groups enables ionic charge to be attached (CPDs) to the periphery of the macromolecule, leading to changes in solubility, and opening the possibility of interaction with other ionic units (energy acceptors) or among the different branches of the individual dendrimers.

During this grant cycle, we have utilized time resolved fluorescence spectroscopy to investigate the photophysics and exciton transport in π-conjugated dendrimers. The following key points have been investigated in this work:

- The presence of multiple equivalent chromophores leads to delocalization of the exciton (an entropy driven process), which we follow using femtosecond anisotropy measurements.
- The difference in the potential energy surfaces of ground and excited state leads to vibronic excitation, which is investigated measuring the ps vibrational cooling in flexible dendrimers.
- Steady-state and time-resolved measurements are used to probe the H-aggregate formation in the first generation ionic dendrimers (CPDs).
- Association of the ionic CPDs with ionic dyes combined with nanosecond time resolved fluorescence anisotropy provides information about the dendrimer size.
- As core chromophores are changed, an energy gradient is created. We use fs-to-ps

spectroscopy to follow the energy transfer through the gradient.

- Comparison of dynamics in the ester protected forms with those of the ionic CPD analogues allows us to understand the effect of conformational changes in the efficiency of the energy transfer.

3.2. Ultrafast Emission Anisotropy Decay and Vibrational Cooling in Conjugated Dendrimers

Emission anisotropy decays in the femtosecond time-scale provide valuable information about exciton dynamics. Since loss of anisotropy due to the rotation of molecules occurs on the nanosecond time-scale, it is possible to characterize other processes without interference from rotational diffusion. In the femtosecond time-scale, the depolarization of the fluorescence signal is related to exciton delocalization and transport. An ultrafast up-conversion instrument was used to explore the excited-state dynamics of two generations of ester protected dendrimers (**Ph-PG-1** and **PG-3**, Scheme 1) in THF. Parallel and perpendicular fluorescence intensities and the anisotropy corresponding to the first 5 ps are shown in Figure 8. The average residual anisotropy obtained for **Ph-PG-1** is 0.12, consistent with its planar C_3 symmetry (planar molecules having C_3 symmetry are expected to have 0.143 residual anisotropy).[36] The measured planarity is confirmed by the molecular dynamics simulations which show a planar structure, even in the presence of the bulky end-groups (see section 2.2). A 330 fs time-component of the anisotropy decay is assigned to energy delocalization among the phenylene ethynylene units of the planar dendrimer configuration. Third generation dendrimer **PG-3** shows an average residual anisotropy of only 0.05, with an ultrafast decay component (~260 fs). As expected, the larger dendrimer is not planar. The non-zero residual anisotropy indicates that **PG-3** has neither a perfectly spherical nor planar shape; the bulky end-groups force the dendrimer to adopt a more globular structure. Exciton delocalization is faster for **PG-3** than **Ph-PG-1**. The third generation dendrimer is larger and many more groups can participate in the delocalization process providing an entropic contribution to the delocalization.

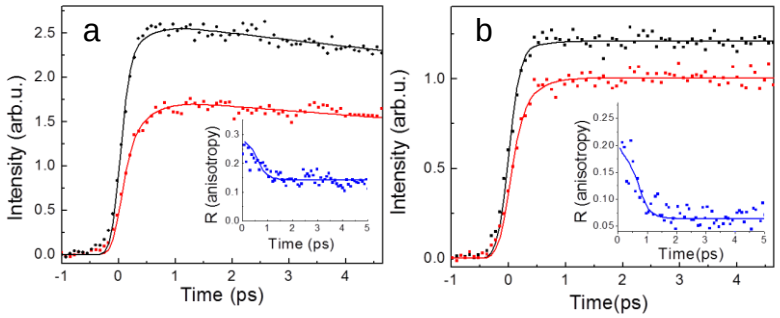

Figure 8: Time-resolved anisotropy for a) **Ph-PG-1** and b) **PG-3** in THF at parallel polarization (black dots) and perpendicular polarization (red dots). Fittings are given in solid lines. The calculated anisotropy data (blue dots) and fits (blue line) are given in the inset.

A shallow ground state potential energy surface is characteristic of phenylene ethynylene containing chromophores. In the excited state, a much steeper potential is expected. Upon fs excitation, this difference in potential surface curvature is reflected in the early time fluorescence dynamics for the first generation dendrimers that lack an energy gradient. For example, the emission arising from early picosecond excited-state dynamics of the dendrimer **Ph-PG-1** shows a marked dependence on detection wavelength which we ascribe to vibrational cooling. The dynamics are observed as a 3 ps component with fractional amplitudes that vary with emission

wavelength (see Figure 9). The contribution from this component is positive at short detection wavelengths and it becomes negative at longer detection wavelength indicating a rise in the population of the emissive state.

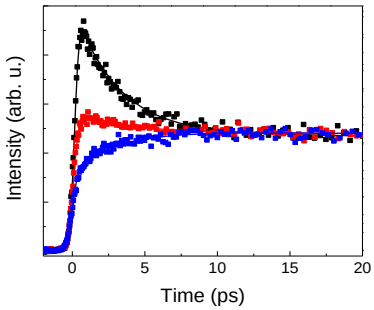

Figure 9. Vibrational cooling observed for **Ph-PG-1** dissolved in THF; detected at 363 nm (black), 376 nm (red) and 420 nm (blue) following excitation at 316 nm.

3.3. H-Aggregates in First Generation CPDs

The first generation ionic CPDs exhibit a particular behavior, which is believed to be related to their planar geometry. The ester-protected dendrimers are well solvated in THF, but when the ester peripheral groups are replaced by carboxylates in the ionic CPDs, the amphiphilic nature of the dendrimers affects their solvation. In the globular 2nd and 3rd generation CPDs the aromatic hydrocarbon core segments are protected by the ionic periphery and thus those dendrimers are well solvated in methanol and water. For the first generation ionic CPDs, the aromatic hydrocarbon segments are exposed to the solvent, and in polar solution the unfavorable solvophobic interactions lead to the formation of aggregates. The optical spectra indicate formation of face-to-face H-aggregates; the large hypsochromic shift of the maximum absorbance wavelength is an indication of an interchromophore angle larger than 30° (see spectra in Figure 10 and cartoon in Figure 11). The formation of H-aggregates by the first generation CPDs is additionally supported by dynamic light scattering measurements,[19] which reveal an increased hydrodynamic radius, and by time resolved data that shows a decrease in the fractional amplitude contributions from ultrafast processes with an increase in the slow components (see Figure 10). Slower decays at longer wavelengths are characteristic of fluorescence decays of aggregates.

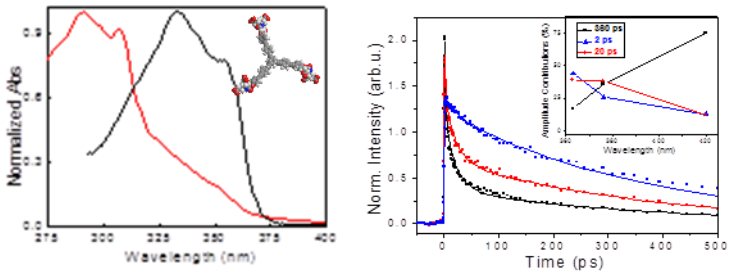

Figure 10: Left: Absorption spectra of first generation dendrimers: **Ph-PG-1** in THF (black) and **Ph-G-1** in methanol (red). Right: Time-resolved emission detected at different wavelengths showing increase contribution from slower components at long wavelength.

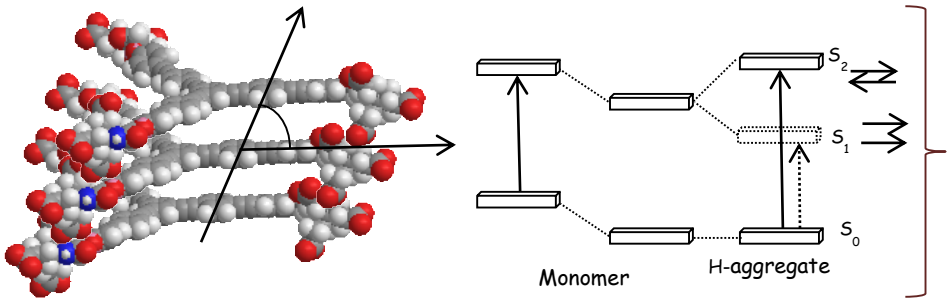

Figure 11: Cartoon showing possible structure of the H-aggregate formed by **Ph-G-1** and the energy levels of the monomers and aggregates.

3.4. Dynamics of Intra-Dendrimer Energy Transfer: Th-PG-n/Th-G-n and Ph-PG-n/Ph-G-n Series

Incorporating different chemical conjugated units into the dendrimers allows us to modulate the energy of the HOMO-LUMO transitions, and create an electronic and spatial energy funnel that drives exciton transfer from the dendrimer periphery to the core. The strength of the coupling between conjugated segments defines the mechanism and dynamics of energy migration: in the presence of an energy gradient, incoherent coupling among chromophores leads to ultrafast exciton transfer towards a sink overcoming the entropic delocalization observed for dendrimers without a gradient.

In the course of our work we have applied steady state and femtosecond fluorescence upconversion spectroscopy to probe the dynamics of the gradient-driven energy transfer in the set of thienylene-containing dendrimers (**Th-PG-n**/**Th-G-n**) and the set of phenylene ethynylene dendrimers with segments of different conjugation length (**Ph-PG-n**/**Ph-G-n**). In these fully conjugated dendritic structures, the peripheral chromophores consist of all meta-linked phenylene ethynylene units. These chromophores are weakly conjugated with the core chromophores, which feature a more extended conjugation (Ph-series) or a thienylene unit (Th-series), both of which reduce the HOMO-LUMO gap. Thus, the structures can be considered as featuring an array of 6 (gen-2) and 18 (gen-3) PE "antenna" units in the dedrimers' periphery, surrounding the lower gap core chromophores. Thus, for these high generation dendrimers we observe two distinct electronic transitions spatially localized at the core and periphery (see Figure 4 on p. 9). The absorption contributions from the core and periphery chromophores units are well separated allowing selective excitation of particular transitions. The steady state fluorescence of all of the dendrimers arises from the core chromophores (see Figure 4 on p. 9). The energy-transfer efficiency from periphery to core (calculated from excitation and absorption spectra) shows a quantum yield > 90% for the ester protected forms in THF.

The dynamics results obtained for the thienylene-containing series are presented first. Two key processes are observed in the fluorescence dynamics (Figure 12). Depending on the excitation wavelength, we observe an intramolecular relaxation pathway or the energy transfer from periphery to core. The relaxation process can be studied in the first generation structures (**Th-PG-1**/**Th-G-1**) and it is seen to exhibit comparatively slow dynamics, ~44 ps in **Th-PG-1**/THF and ~7 ps in **Th-G-1**/methanol. To understand the periphery-to-core energy transfer, we looked into very early time scales (up to 5 ps) with improved experimental time-resolution, focusing on the 2^{nd} and 3^{rd} generation structures. The up-conversion results show a clear signature for the energy transfer in the form of a fast decay component ($\tau < 4$ ps) at short wavelength combined with a rise component at longer wavelengths (Figure 12).

To understand the influence of the ionic periphery in the CPDs on the dynamics of the periphery-to-core transfer, we compare energy-transfer rates and efficiencies for the Th-containing dendrimers. Interestingly, the results find that in the ionic CPDs (**Th-G-n**) transfer is faster than for the ester protected forms (**Th-PG-n**). This is likely due to collapse of the dendrimer structure in the ionic CPDs leading to shorter distances and stronger interactions between periphery and core chromophores. The energy-transfer efficiency, as assessed by comparing absorption and emission excitation spectra, is slightly decreased (from 93% to 81% and from 99% to 65% for

the 2nd and 3rd generation, respectively) due to intra-molecular interactions. The excitations localized over the outer parts of the dendrimers are believed to relax to trap states (k_{trap}= (7 ps)$^{-1}$) and not reach the core part leading to lower efficiencies and faster rates. Assuming weak coupling between chromophores, computed interaction energies are on the order of 40-60 cm^{-1} for the ester analogues, increasing to 130-150 cm^{-1} for the ionic CPDs in methanol (see Figure 14 below).

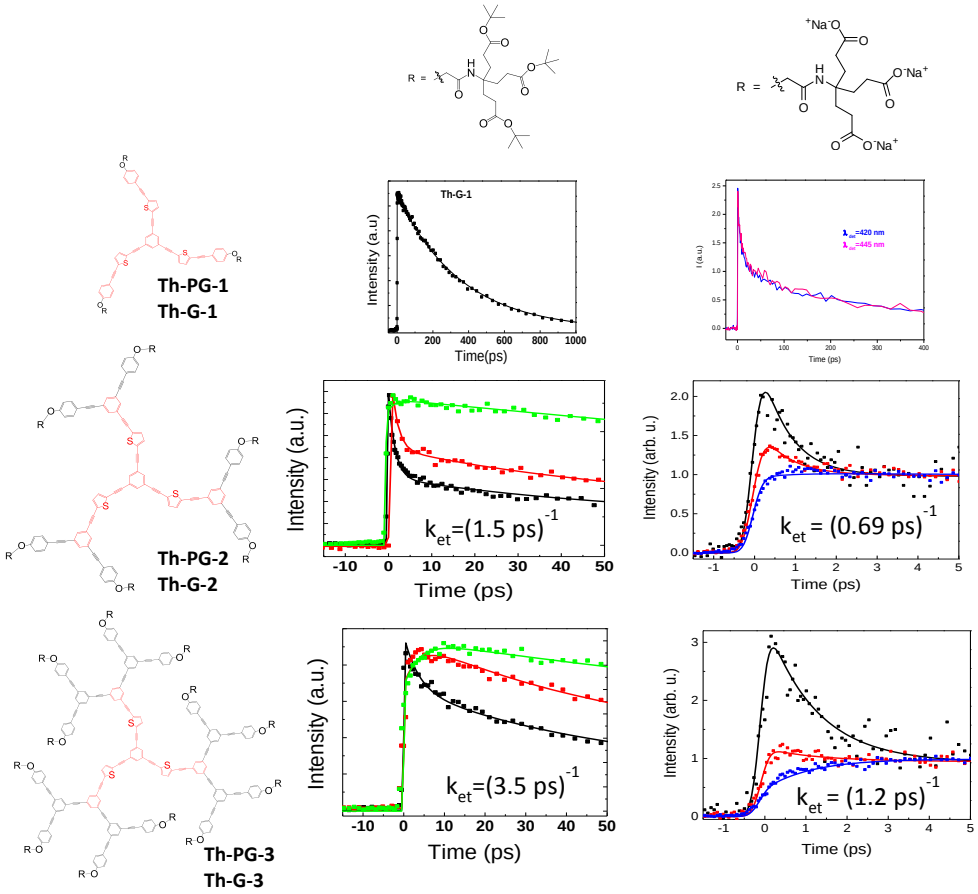

Figure 12. Dynamics of intra-dendrimer energy transfer in **Th-PG-n** (THF, middle column) and **Th-G-n** (methanol, right column) as determined by fluorescence upconversion spectroscopy. Different colors represent emission kinetics monitored at different wavelengths. Rates are computed from global fit of the data at all wavelengths. The transfer dynamics are faster for the 2nd generation compared to the 3rd and overall faster in the ionic CPDs.

The same fluorescence upconversion dynamics studies were performed for the set of phenylene core dendrimers, **Ph-PG-n** and **Ph-G-n** (Figure 13). These systems show qualitatively similar behavior as described above for the thienylene series, with a few important differences. First, overall the periphery-to-core transfer is faster for the **Ph-PG-n**/**Ph-G-n** series compared to the corresponding **Th-PG-n**/**Th-G-n** structures. Second, the transfer is only modestly faster in the ionic CPDs, **Ph-G-n**, compared to the ester protected forms, **Ph-PG-n**. Overall, these findings point to the fact that the periphery-to-core interaction energies are larger in the phenylene series of dendrimer structures.

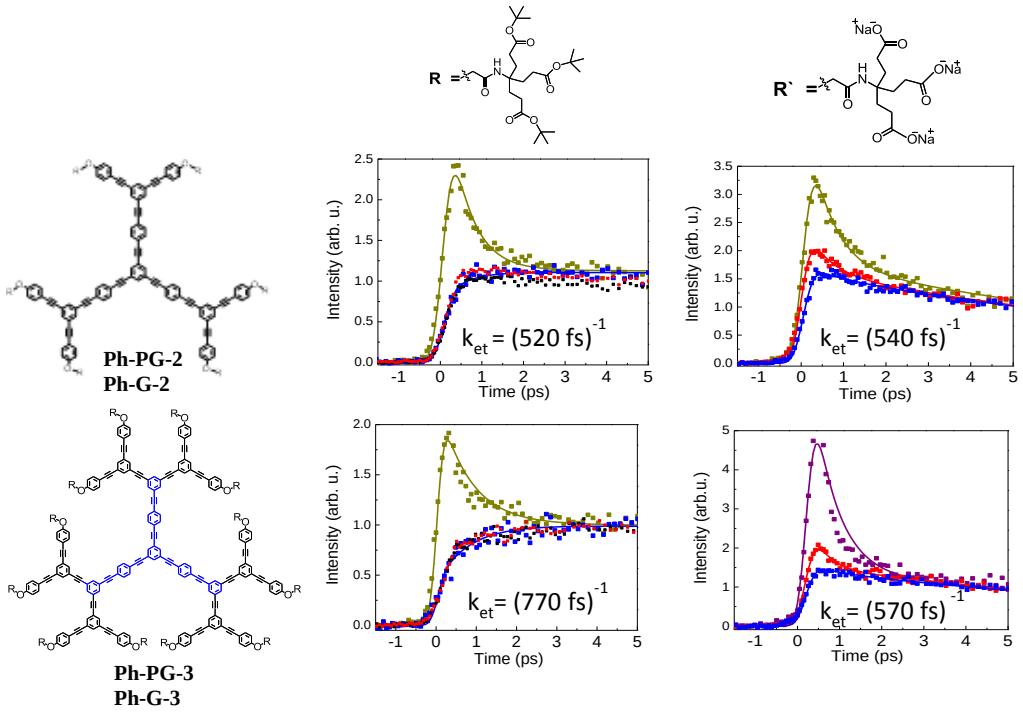

Figure 13. Dynamics of intra-dendrimer energy transfer in **Ph-PG-n** (THF, middle column) and **Ph-G-n** (methanol, right column) as determined by fluorescence upconversion spectroscopy. Different colors represent emission kinetics monitored at different wavelengths. Rates are computed from global fit of the data at all wavelengths.

The experimental energy transfer rates for the **Ph-PG-n**/**Ph-G-n** and **Th-PG-n**/**Th-G-n** series have been used to calculate interaction energies between donor (periphery) and acceptor (core) chromophores, and to check the validity of the Förster model for these dendrimers. In general, the interaction energies are less for the third generation of the ester forms due to the longer distance between periphery and core. In addition, overall the values obtained are relatively large, which makes the weak coupling limit assumption questionable for these compounds. Comparison with values obtained using Förster theory (which assumes very weak coupling and point-dipole interactions) shows the breakdown of those assumptions leading to the conclusion that the energy transfer depends greatly on the shape and size of the interacting transition dipoles.

In summary, our studies on energy transfer in this family of conjugated (polyelectrolyte) dendrimers allow us to compare the energy transfer rates and interaction energies for phenylene (**Ph-PG-n**/**Ph-G-n**) and thienylene (**Th-PG-n**/**Th-G-n**) extended dendrimers in the ester and ionic forms. The energy-transfer rates are slower for higher generations due to

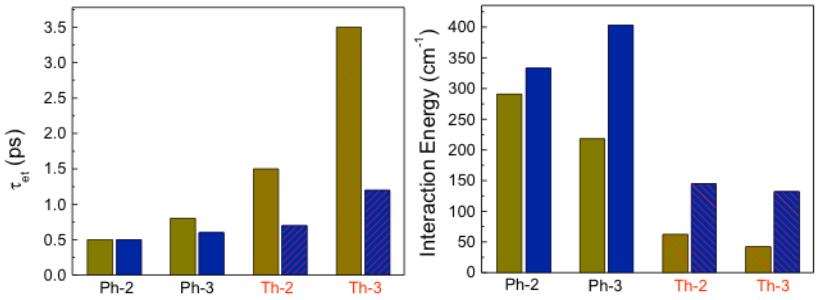

Figure 14. Comparison of energy-transfer rates and interaction energies in the **Ph-PG-n**/**Ph-G-n** and **Th-PG-n**/**Th-G-n** dendrimers. Left panel compares the observed dynamics and right panel compares the computed interaction energies. Brown bars represent the ester forms (**Ph-PG-n**) and blue bars are the ionic forms (**Ph-G-n**).

longer distance between donor and acceptor units. The energy-transfer rates are faster in the ionic CPDs, which is attributed to the partial collapse of the CPD structure due to solvophobic forces. Th-dendrimers have slower energy-transfer rates and they are more flexible. The faster energy transfer rates in the ionic forms are even more pronounced for the Th-dendrimers. This can be caused by collapse of these dendrimers after the introduction of ionic end groups.

4. CPE Aggregation Studied by Fluorescence Correlation Spectroscopy

In very recent work we have developed Fluorescence Correlation Spectroscopy (FCS) as a new approach to study interactions in conjugated polyelectrolyte solutions.[18] We plan to continue to apply this method in the proposal; in the progress report we provide a brief introduction to the technique and some of the results that have been obtained to date using FCS.

FCS is a statistics based analytical technique first reported by Madge, Elson and Webb.[37] It monitors the spontaneous fluctuations of fluorescence intensity of diffusing molecules within a small excitation/emission volume (~femtoliter) created by focusing a single mode laser with a confocal fluorescence microscope. Various processes including Brownian diffusion, chemical reaction or flow contribute to the fluorescence intensity fluctuation. By applying an autocorrelation function $G(\tau)$, the raw fluctuation data is converted to a decay curve, which can be analyzed using an appropriate fitting model. In our investigations the correlation decay time is associated with the diffusion time of the fluorescent CPEs, and this is related to the size (molecular weight) of the polymer or polymer aggregate in solution. FCS has been primarily employed for the analysis of biological systems.[38-40] However, there are a few previous studies which have used FCS on CPEs, and of most interest in this work are studies by Waldeck[41] and Wang[42] which have investigated the solution properties of water soluble conjugated polyelectrolytes by using FCS.

In the past year, we have established a facility in our labs that allows the routine measurement of FCS correlation curves with excitation at 405 nm and detection for $\lambda > 450$ nm. This system is ideally suited for the study of the phenylene ethynylene based CPEs that are the focus of the DOE program. Here we describe a set of recent studies which have correlated the fluorescence quenching of an anionic CPE by metal ions with the ion-induced aggregation as monitored by FCS. This work is fully described in a paper that is in the final stage of revision before it is submitted for publication. This work has used **PPE-^{d}CO$_2^-$** (Figure 15) which has been previously shown to exist in a molecularly dissolved state in aqueous solution.[10] In this work we have explored the effect of addition of a series of mono- and polyvalent metal cations on the fluorescence and the FCS properties of the solutions. In particular, Figure 15 shows the FCS correlation curves for **PPE-^{d}CO$_2^-$** in solution with 15 μM of various metal ions. The results show that the monovalent ions and Ca^{2+} have little or no effect on the diffusion time. By contrast, the polyvalent transition metal ions Cu^{2+}, Fe^{2+} and Fe^{3+} have a marked effect on the diffusion time (note the shift of the correlation curves to longer time in Figure 15a). The results show that the latter metals are able to induce formation of relatively large polymer aggregates, presumably by forming ionic/covalent crosslinks via binding to carboxylate groups of different polymer chains. The plots in Figures 15b and c show that there is a correlation between the Stern-Volmer fluorescence quenching and the metal-ion induced increase in FCS diffusion time. Specifically, the fluorescence quenching plots for Cu^{2+}, Fe^{2+} and Fe^{3+}exhibit a pronounced

upward curvature that turns on at ~5 μM. Interestingly, this is the same metal ion concentration where the FCS diffusion time begins to increase significantly. These results provide direct evidence for the strong correlation between the amplified fluorescence quenching effect and the ion-induced aggregation which has been postulated mainly on the basis of indirect evidence from absorption and fluorescence spectroscopy.[27,28,32]

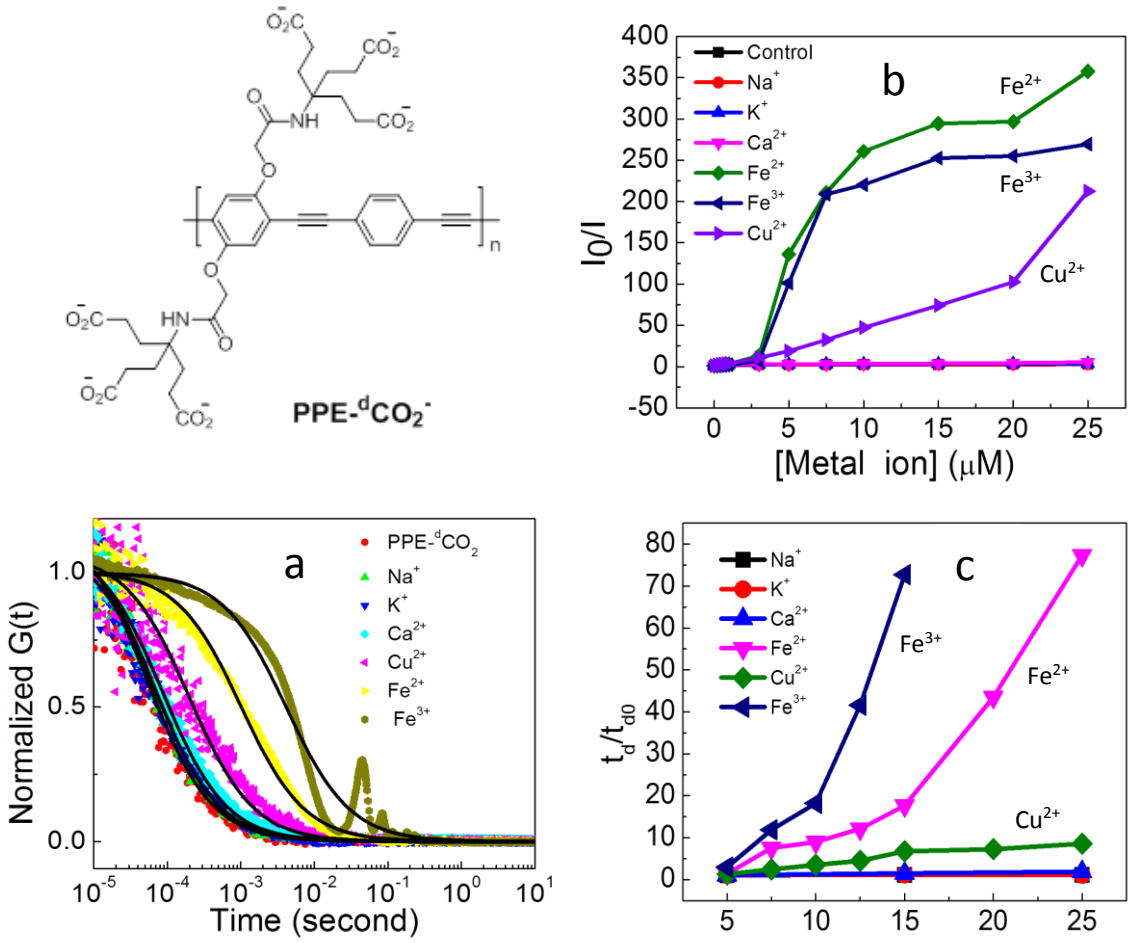

Figure 15. Results of combined metal ion-fluorescence quenching and fluorescence correlation spectroscopy study on **PPE-$^{d}CO_2^-$** (structure at upper left). a) Correlation curves from FCS, polymer concentration 780 nM and metal ions at 15 μM. Shift in the correlation plot to right indicates a longer diffusion time (t_d), indicating an increase in CPE aggregate size. b) Stern-Volmer quenching of **PPE-$^{d}CO_2^-$** by metal ions. c) Relative change in FCS diffusion time (t_d/t_{d0}) for addition of metal ions to **PPE-$^{d}CO_2^-$**.

5. Donor-Acceptor Ions: Structures and Synthesis

5.1. Donor-Acceptor Conjugated Polyelectrolyte Oligomers

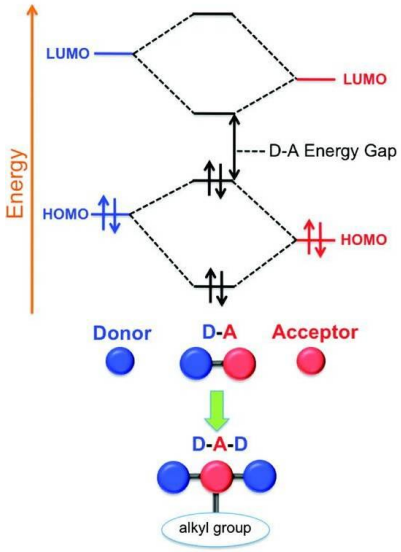

Figure 16. Energy level diagram of a D–A system with a reduced HOMO–LUMO gap.

Hybrid solar conversion utilizing nanostructured metal oxide thin films has exceeded 11% efficiency when employing transition metal coordination complexes,[43,44] though much effort is now directed toward finding metal-free, all organic dye sensitizers to harvest solar photons.[45,46] To date, reported compounds have relied on donor-acceptor (D-A) type architectures where the molecule is aligned in a dipolar sense with a single donor supplying electron density to a single acceptor, which is positioned close to the metal oxide film through a carboxylate linkage. An illustration of the D-A concept is depicted in Figure 16 where the HOMO of the donor and the LUMO of the acceptor are largely responsible for the location of the frontier orbital energy levels in the conjugated system. In our research, we have furthered this concept by using donor-acceptor-donor (D-A-D) type molecules and polymers that are known to have absorption bands extending into the red and near IR regions of the spectrum, a highly desirable feature ensuring maximum absorption of the solar spectrum.

We initiated our investigation using 1,2,3-benzotriazole (**BTz**) because of its feasibility for alkylation at the central nitrogen, along with recent reports suggesting that in polymer systems it acts as an electron deficient, and therefore electron accepting, building block.[17] However, when used as an acceptor in thiophene based oligomeric systems, the LUMO is sufficiently high that the absorption band is largely localized in the UV-region of the spectrum. Other well-known acceptors, such as 2,1,3-benzothiadiazole (**BTD**), have desirable, low energy LUMO levels, but they cannot be modified to include carboxylate adsorption units. We have, therefore, developed a novel acceptor that is a hybrid of **BTz** and **BTD**, benzo(triazole-thiadiazole) (**BTzTD**) which absorbs visible light and also supports *N*-functionalization. A conceptual picture of this hybrid acceptor concept is presented in Figure 17.

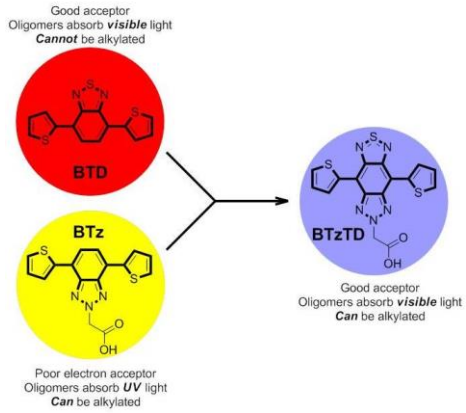

Figure 17. Molecular structures of trimers containing thiophene donors and benzothiadiazole (BTD), benzotriazole (BTz), or BTzTD acceptor units.

Throughout this grant cycle, we have accomplished a full study of D-A-D type molecular structures that are designed to bind to and sensitize wide bandgap metal oxide semiconductors. Scheme 3 outlines the target D-A-D triads (structures **O1** and **O2**). The acceptors **BTz** and **BTzTD** were flanked with either (**a**) thien-2-yl, (**a'**) 5-methylthien-2-yl or (**b**) 5'-methyl-2,2'-

bithien-2-yl groups to determine how the strength of the donor influences the resulting frontier orbital energies and redox properties of the D-A-D oligomers and affects the resulting relaxation dynamics after photexcitation. These compounds were further functionalized at their central N-atom with *tert*-butylacetate which is easily cleaved with trifluoroacetic acid as catalyst, thus releasing isobutylene and regenerating the free carboxylic acid for further adsorption onto metal oxide surfaces.

Scheme 3. D-A-D triads **O1** and **O2**

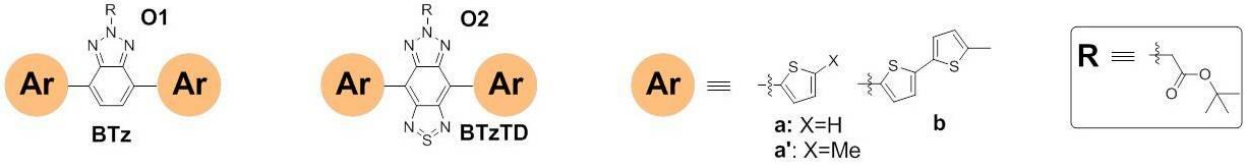

These D-A-D triads were subjected to a detailed study based on electrochemical and spectroscopic methods, coupled with DFT calculations. It was found that their electron affinity was unexpectedly low which rendered **BTz** as electro-neutral. This case is contrary to previous reports where **BTz** is used as an electron acceptor to afford polymers that absorb visible light.[47,48] Our results, compared with those derived from analogue structures based on **BTD**, point toward the importance of the central atom (i.e., N vs. S) in the distribution of the frontier orbital energies which impacts the electron accepting ability of the chromophore and, ultimately, its electronic properties. The fusing of the **BTz** and **BTD** into one convergent unit results in a large stabilization of the LUMO and a slight destabilization of the HOMO energy which, consequently, narrows the optical gap of the **BTzTD**-based chromophores (Figure 18). This LUMO stabilization also leads to a different dominant excited state deactivation mechanism after photoexcitation from **BTz**-based systems. The **BTzTD** hybrid acceptor, having elements of both **BTz** and the stronger acceptor **BTD**, maintains the ability for alkylation while increasing electron accepting ability of the overall conjugated system. Thus, interesting opportunities toward adsorption onto metal oxide surfaces are envisioned in which the harvesting of low

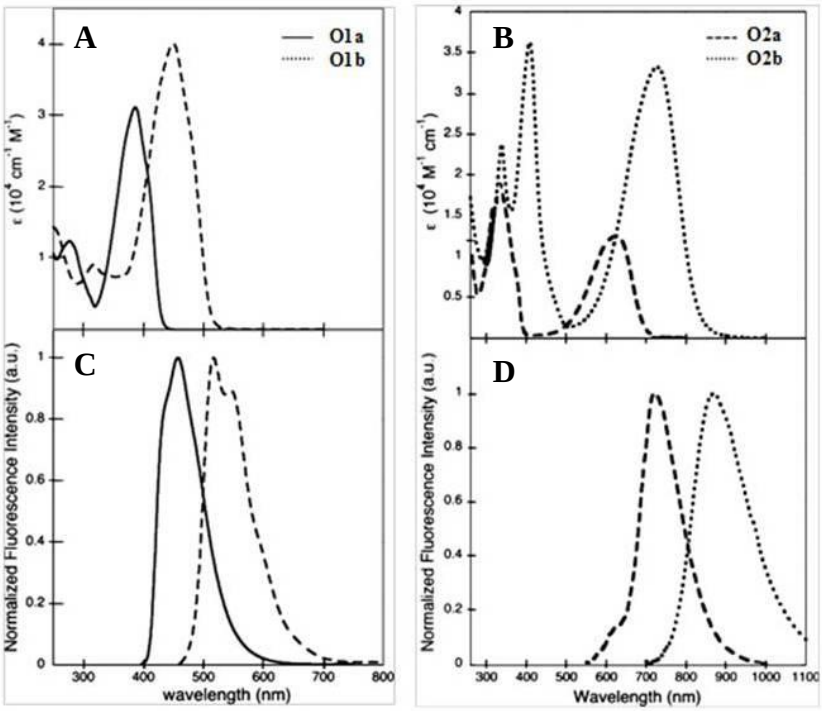

Figure 18. UV-Vis absorption (**A,B**) and fluorescence spectra (**C,D**) of **BTz** (**O1a** and **O1b**) and **BTzTD** (**O2a**, **O2b**) oligomers in dichloromethane. Note the difference in the wavelength axis scales in panels A and C vs. that used in panels B and D.

energy photons from the visible spectrum is available. A comprehensive spectroscopic and electrochemical study is described in Section 5.2, below, along with theoretical remarks.

Subsequent to this work, we extended our studies to fused D-A chromophores where anchoring sites can be incorporated to bind metal oxides through the acceptor unit. Specifically, we used phenanthrene and benzodithiophene as donors based on their availability and well known properties.[49,50] For the acceptors, we focused on phenazine (**Pz**), which is easy to functionalize with esters for subsequent adsorption onto metal oxides. In this study, 2-methylthiophene (MT) and 3-hexylthiophene (HT) were employed as chain extending donors. Using this concept, we prepared the dibenz[a,c]phenazine (**DBP**) and dithieno[a,c]phenazine (**DTP**) family of compounds having the structures as illustrated in Figure 19. While in most cases the flanking thiophene units bear pendant hexyl chains to enhance solubility and decrease aggregation, compounds **DTP-3** and **DTP-4** incorporate α-methyl groups to block any cation radical coupling that may occur upon electrochemical oxidation. By structurally comparing **DBP** and **DTP** derivatives, it is evident that the position of the terminal coupled thiophenes leads to various conjugation pathways along the π-systems. Each of the compounds are mono-ethyl ester substituted which are easily hydrolysable to yield the carboxylic acid derivatives desired for metal oxide adsorption.

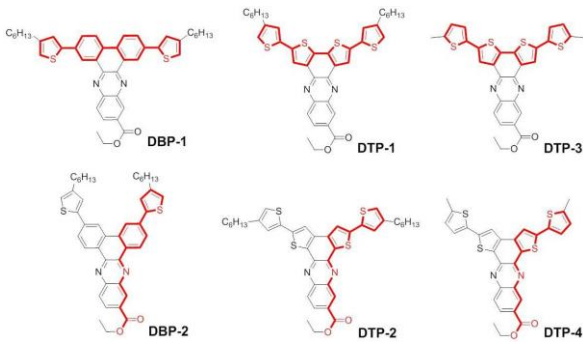

Figure 19: Molecular structures of dibenz[a,c]phenazine DBP (**1,2**) and dithieno[a,c]phenazine DTP (**3-6**). In red, conjugation pathways are highlighted

The optical properties of the **DBP** and **DTP** compounds were investigated in toluene, where the absorption profile depended considerably on the pattern of substitution (Figure 20). Absorption bands at ~ 290-350 nm and ~ 400-440 nm are observed for **DBP** compounds with strong light absorption at λ > 400 nm ($\log(\varepsilon_{abs})$ ~ 3.70-4.40 at λ_{max} above 400 nm). The **DTP** compounds exhibit red-shifted absorption bands with similar absorptivity as the **DBP** derivatives at λ > 400 nm ($\log(\varepsilon_{abs})$ ~ 3.81-4.06 for **DTP-4** at λ_{max} above 400 nm). The inclusion of thienyl units fused within the phenazine core mainly raises the HOMO energies, narrowing the optical gap. For all compounds the lower energy bands correspond to charge transfer transitions. We speculated that the enhanced oscillator strengths of **DTP-1/3** compared with **DBP-1** are due to a more planar conjugated structure given the lower steric demands that thiophene has compared to benzene. All

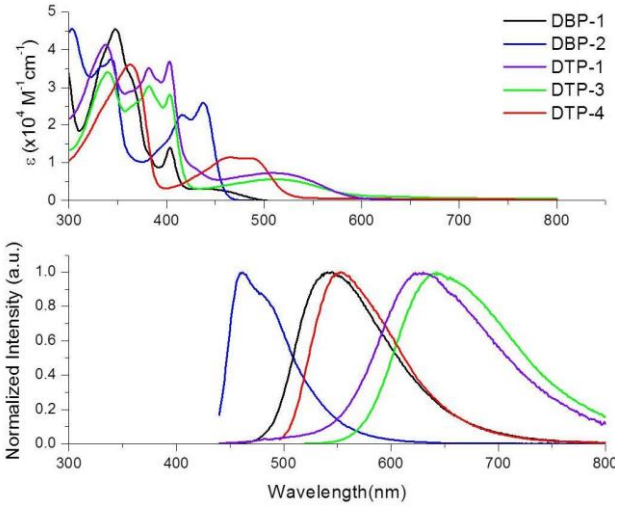

Figure 20. Absorption (*top*) and normalized emission (*bottom*) spectra of **DBP** and **DTP** derivatives.

compounds fluoresce with emission maxima at λ > 440 nm, where **DTP**-based compounds show red-shifted emission with respect of their **DBP** analogues.

5.2. Properties of Donor-Acceptor Ion Systems

5.2.1. The Role of the Central Atom in BTz, BTD, and BTzTD Derivatives

Initially, the **BTz** unit was envisioned as an electron acceptor in oligomeric systems given that it bears electron-accepting diimine groups as part of its benzannulated structure; however, our theoretical and experimental results provide us with a significantly different picture.

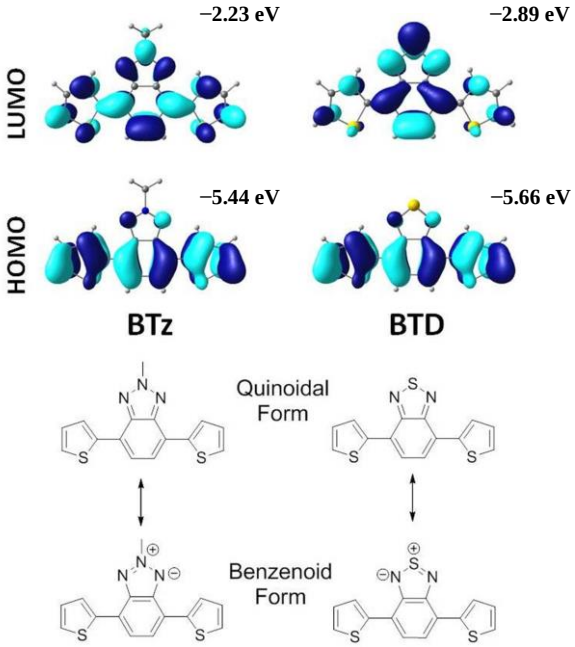

Figure 21. Frontier orbital isodensity maps and energies of BTz and BTD flanked with thienyl groups.

We compared the **BTz** oligomer **O1a** (recall Scheme 3 for compound labeling) and its **BTD** analogue by computing their frontier orbital energies in vacuum (Figure 21), where the pendant *tert*-butylacetate was replaced with methyl to reduce computation time. The computed LUMO energies are −2.23 eV and −2.89 eV for the for the **BTz** and **BTD** models, respectively, which highlight that the identity of the central atom (N and S in **BTz** and **BTD**, respectively) substantially impacts the LUMO level of the oligomer. The LUMO picture reveals a quinoidal form with contribution of the thienyl units in both systems, where such contribution is reduced in the case of the **BTD** model. The variation of the HOMO energies followed the same trend, yet the energetic difference is not as large. By comparing bond lengths and Wiberg indices[51] between acceptor units, we see that the quinoidal form is more prominent for **BTz** than for **BTD** which suggests that the aromaticity of the benzene ring is an important factor in determining the electron affinity. Natural population analysis (NPA) of both models is consistent with this picture. The formal charges of both imine nitrogens are strikingly different for both systems: in **BTz**, these formal charges are −0.272 while for **BTD** they are −0.611. This difference is even greater for the central atom where the N-CH_3 bears a formal charge of +0.066 while the sulfur formal charge is almost unity (+0.877).

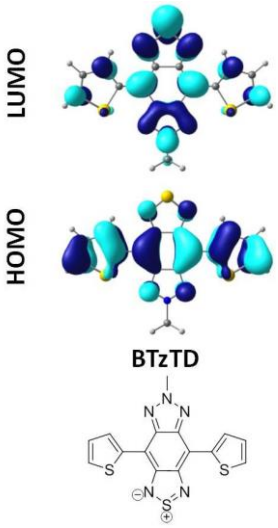

Figure 22. Frontier orbital maps of model BTzTD oligomer.

The thiadiazole unit mainly affects the LUMO distribution of the fused **BTzTD** system as judged by the analysis of the calculated isodensity maps of the frontier orbitals of an analogous **BTzTD** model (Figure 22). The effect that this transformation has on the HOMO energies is smaller. The NPA of the charge distribution on individual atoms of the **BTzTD** reveal that sulfur bears a

formal charge of +0.912, while the thiadiazole nitrogens have formal charges of −0.627. In contrast, the N−CH_3 nitrogen has a formal charge of +0.089, while the triazole nitrogens have computed formal charges of −0.273. This is consistent with the bigger orbital lobe found in the sulfur atom than in the nitrogen atom in the LUMO.

Our spectroscopic and electrochemical data suggest that **BTz** acts more as an electron neutral, rather than electron accepting moiety in oligomeric systems. In oxidative electrochemical studies, oligomers **O1a'** and **O2a'** were used instead of their non-methylated versions in order to avoid radical-radical couplings. Reduction processes are centered at −2.44 V for **O1a** and −2.23 V for **O1b** against the $Fc|Fc^+$ redox couple in THF, reflecting the lack of electron accepting ability of the central **BTz** unit. Oligomer **O1a'** shows an irreversible oxidation wave with an onset at approximately +0.42 V by CV (+0.38 V by DPV) and oligomer **O1b** shows a quasi-reversible oxidation centered at 0.25 V (onset of oxidation at 0.20 V by CV and 0.12 V by DPV). The **BTzTD** oligomers exhibit lower oxidation potentials when compared to their **BTz** analogues: compound **O2a'** has a reversible oxidation with $E^{1/2}_{ox}$ of +0.38 V vs. $Fc|Fc^+$ (onset at +0.22 V by CV and +0.13 V by DPV) and compound **O2b** shows quasi-reversible oxidation at a lower potential centered at +0.20 V vs. $Fc|Fc^+$ (onset at +0.05 V by CV and −0.07 V by DPV). Also, both **BTzTD** oligomers show lower reduction potentials than the **BTz** oligomers: both **O2** compounds show reversible reductions with $E^{1/2}_{red}$ values of −1.37 and −1.26 V, respectively. The onset of reduction for **O2a** is −1.27 V by CV (1.20 V by DPV), while the onset for **O2b** is −1.23 V by CV (−1.15 V by DPV).

To further characterize the optical properties of the oligomers, we explored the solution-phase excited-state dynamics for the **BTz** and **BTzTD** oligomers. All the oligomers show fluorescence with moderate to high quantum yields. Fluorescence lifetime measurements reveal that **BTz** oligomers **O1a-b** have lifetimes (τ_f) in the range of 1–2 ns. The radiative decay rates for these range around (2-3) × 10^8 s^{-1} and the non-radiative rates range around (3-7) × 10^8 s^{-1}. These lifetimes and radiative decay rates are typical for π-conjugated oligomers with strongly allowed long-axis polarized π–π* singlet excited states. Furthermore, fluorescence competes effectively with non-radiative events as main deactivation pathway from the S_1 state. By contrast, the **BTzTD** oligomer **O2a** has a fluorescence lifetime that is 1 order of magnitude larger than the **BTz** series compounds ($\tau \approx 10$ ns), and the corresponding radiative rate is significantly less (6 × 10^7 s^{-1}). The non-radiative decay rate, however, is significantly higher (4 × 10^8 s^{-1}) than the radiative decay for this case. Also notable is the fact that the fluorescence quantum yield for **O2b** is markedly less than for the other oligomers, yet the fluorescence lifetimes are comparable to that of **BTz** oligomers. This effect is likely due to the energy gap law, where the nonradiative decay rate is increased due to the relatively low energy of the singlet excited state in this oligomer. In terms of kinetic events, the radiative decay ranges around (1-5) × 10^7 s^{-1} while the non-radiative decay is evidently faster, (2-8) × 10^8 s^{-1}.

Given the dominant non-radiative rates for many of the oligomers of this study, nanosecond–microsecond transient absorption spectroscopy was carried out for samples in degassed THF solution at room temperature to characterize the triplet state for the series of **BTz** and **BTzTD** oligomers. **BTz** containing oligomers exhibit strong transient absorption in the mid-visible region following 355 nm excitation (Figure 23), assigned to the triplet–triplet absorption (TTA) of the lowest triplet state based on O_2 quenching experiments. The TTA decays with first-order kinetics for both oligomers with lifetimes ranging in the 30–50 μs in Ar-saturated solutions. Increasing the number of thiophene rings in the oligomer system leads to a red-shifted TTA spectrum from 476 to 640 nm and is more intense as observed by comparing oligomers **O1a** and **O1b**. The possibility that the triplet yield is larger in **O1b** as compared to **O1a** is consistent with the observation that the fluorescence quantum efficiency is smaller for the longer oligomer (note that fluorescence and ISC are competing processes, so an increase in one pathway would be reflected by a reduction in the other). In contrast to the **BTz** oligomers, transient absorption spectroscopy of the **BTzTD** containing oligomers reveals no observable TTA. From this observation, we conclude that intersystem crossing in the **BTzTD** oligomers is inefficient due to the significant degree of charge-transfer character of the singlet excited state.

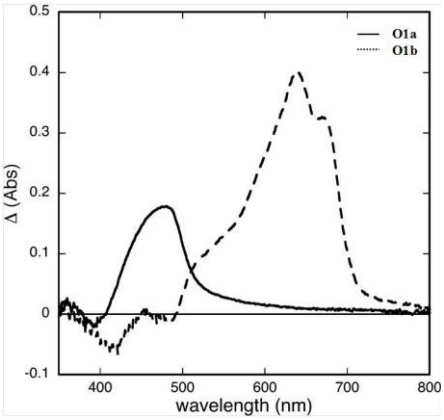

Figure 23. Transient absorption spectroscopy of **BTz** derivatives in THF at room temperature. Spectra obtained at 100 ns delay following a 355 nm, 8 mJ excitation pulse.

5.2.2. Fused D-A Systems: Dipolar DBP and DTP Derivatives

DFT calculations were carried out on **DBP** and **DTP** bis-thienyl acceptors to develop an understanding of the electronic structures of these molecules. The respective isodensity surfaces computed are shown in Figure 24 for the frontier orbitals (the alkyl substituents in the flanking thiophenes were removed to speed the computations). The electron density in the HOMO is centered on the donor backbone for compounds **DBP-1** and **DTP-1**, and across the donor-acceptor unit for compounds **DBP-2** and **DTP-2**. The LUMO is largely confined on the central phenazine unit for all compounds.

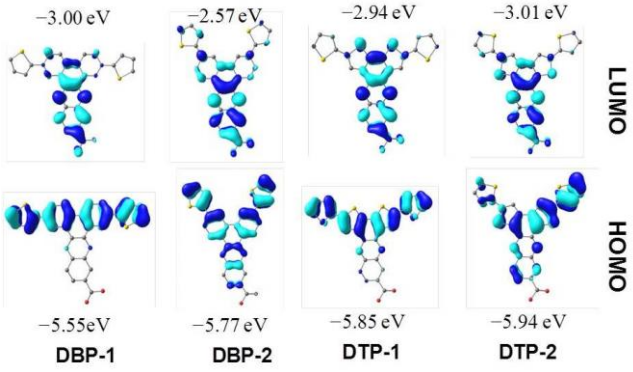

Figure 24: HOMOs and LUMOs representation surfaces of compounds **DBP** and **DTP** derivatives of interest.

To quantitatively examine the frontier orbital energies, we used both cyclic voltammetry (CV) and differential pulse voltammetry (DPV) and assign the half wave potentials versus the $Fc|Fc^+$

redox couple. While all of the donor-acceptor compounds show reversible reductions, they feature irreversible oxidations. For the **DTP-**based compounds, we blocked the terminal α-thienyl positions with methyl groups to suppress the possibility of thienyl coupling (structures **DTP-3,4**). Although the oxidation of these molecules is still irreversible as judged by CV, we were able to obtain the oxidation potentials via DPV. In agreement with theory, all the LUMOs levels are higher than the conduction band of titanium dioxide, indicating an energetically viable electron injection. Furthermore, the trends obtained by our experimental results nicely match those predicted by theory, where the differences in values were more important for the LUMO than for the HOMO.

Examining the photophysical properties of **DBP-1,2** and **DTP-3,4** solutions in toluene shows the Stokes shift to be smaller for compound **DBP-2** (0.15 eV) than the rest of the triads: **DBP-1** (0.63 eV), **DTP-1** (0.46 eV), **DTP-3** (0.50 eV), and **DTP-4** (0.32 eV). This indicates significant reorganization energies of the latter set of compounds upon photoexcitation and correlates well with their lower oscillator strengths as judged by the Franck-Condon principle. We observe a low absorptivity of **DBP-1** at low energies suggesting that vibronic coupling of the donors and the acceptor is weak (i.e. the lowest energy transition is HOMO→LUMO), and the large Stokes shift observed is consistent with this idea. Given that toluene is relatively non-polar, it is expected that most of the contribution to the overall reorganization energy is from the internal reorganization as opposed to solvent dipole reorientation. Finally, the fluorescence quantum yields of **DBP-1**, **DBP-2** and **DTP-1** are moderate which suggests that fluorescence is a competitive mechanism for excited state deactivation in media of low polarity.

6. Studies of Conjugated Polyelectrolytes at Metal-Oxide Surfaces

6.1. Charge Injection at Conjugated Polyelectrolyte/Single Crystal TiO_2 Interfaces.

In order to gain a better understanding of the structure of the CPE films at the metal-oxide interface, and to develop a correlation between the structure of the film, exciton diffusion to the interface and charge injection, we have carried out studies in collaboration with Prof. Bruce Parkinson at the University of Wyoming.[14] These studies are focused on using AFM and photocurrent spectroscopy measurements to study CPE films at well-defined anatase single crystal (sc) TiO_2 interfaces. The nanoscale morphology and photoactivity of conjugated polyelectrolytes (CPEs) deposited from different solvents onto single crystal TiO_2 was investigated with atomic force microscopy (AFM) and photocurrent spectroscopy, using methods that have been established in previous work in the Parkinson lab.[52] This study used nearly atomically flat, single crystal TiO_2 (both anatase and rutile) electrodes as model systems to correlate conjugated polyelectrolyte surface morphology with sensitized photocurrent yields. The CPEs used in this study (Figure 25a) share a common carboxylated dialkoxyphenylene-1,4-ethynylene backbone to facilitate COO-TiO_2 binding, but differ in the alternating arylene ethynylene moiety [2,5-thienyl (TH) or 1,4-benzo[2,1,3]thiadiazole (BTD)] that determines the HOMO-LUMO gap of the material. From the ground state reduction potentials of each CPE, we estimate >0.5 V driving force for photo-excited electron injection from either CPE into bulk TiO_2 (Figure 25b). Despite sufficient thermodynamic driving force for electron injection, the two CPE sensitizers had very different conversion efficiencies when employed as sensitizers in a mesoporous dye-sensitized photoelectrochemical cell.[53] Since electron injection is

thermodynamically favorable at CPE/TiO_2 interfaces, the disparity in the device efficiencies may originate from exciton trapping and recombination due to either poor transport in single polymer chains or between chains or poor electronic coupling between the polymer and the TiO_2 conduction band.

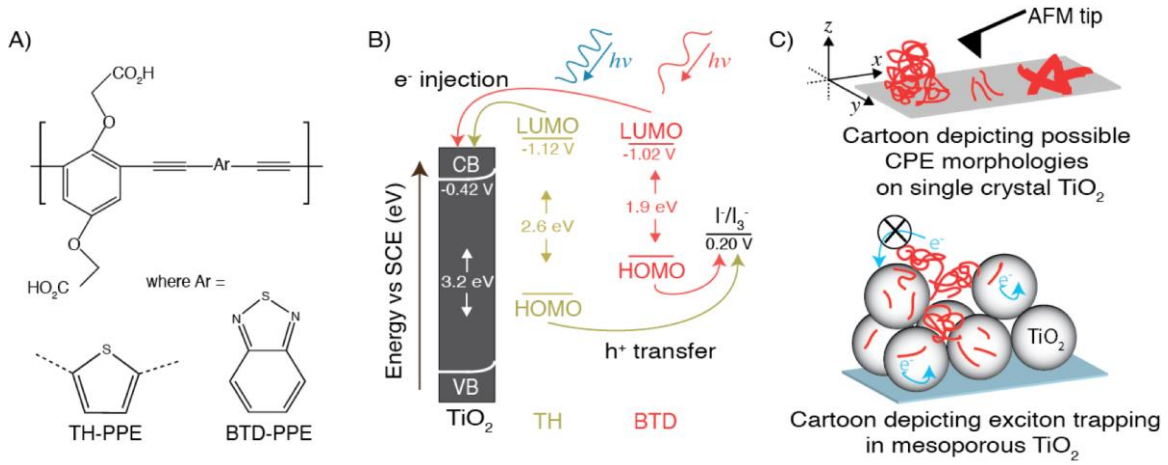

Figure 25. (A) Chemical structures for the conjugated polyelectrolyte sensitizers studied herein. (B) Band energy diagram showing the HOMO-LUMO energy level alignment of each CPE with the anatase TiO_2 conduction and valence bands (CB and VB) at pH 5.5[14]. (C) Representation of possible CPE morphologies (depicted as red lines) on a single crystal TiO_2 substrate (top) and how these variable CPE morphologies may lead to exciton trapping or recombination in mesoporous TiO_2 films (bottom).

Obtaining topographic information of adsorbed CPE species within a mesoporous oxide film is analytically challenging. However flat, single crystal TiO_2 substrates allow for atomic force microscopy (AFM) probes to directly access CPE adsorbates (Figure 25c). A variety of surface-bound polymer species could be present on a planar, single crystal TiO_2 surface due to inhomogeneity of polymer samples that may exhibit broad size distributions or a variety of conformations in the solvated state. Nonetheless we anticipate that the carboxylated polymer backbone facilitates polymer-TiO_2 covalent binding analogous to the binding mechanism for transition metal complex sensitizers. Figure 25c (bottom) shows a cartoon illustration of a mesoporous TiO_2 device depicting how polymer morphology may affect the photo-excited electron injection efficiency. For instance, inefficient exciton transport may occur for aggregated polymer chains whose photogenerated excitons must hop between several polymer chains to reach the TiO_2 interface. Alternatively, individually adsorbed CPE chains are expected to inject electrons more efficiently, especially if they have multiple carboxylate attachments. Deconvoluting the origin of the sensitized photocurrents from CPE conformations (ie. aggregated chains versus isolated chains or many TiO_2 attachments versus few attachments) amongst the multitude of CPE sensitizers is difficult at the buried interfaces in mesoporous TiO_2. In this work we directly determined the interfacial polymer morphology on planar TiO_2 surfaces (as shown in Figure 25c), and correlated structure with electron injection efficiency.[14] Previous studies were limited to indirectly correlating CPE morphology with current-voltage behavior by manipulating device processing conditions such as temperature dependent CPE adsorption,[54] blending versus spin coating,[55-57] or device annealing[55]. Although these procedures may lead to future device improvements, cell efficiencies can be affected by multiple factors and does not

provide information regarding how the CPE morphology directly affects the electron injection yields.

The reviewer is directed to the paper for a full account of this first study;[14] here we provide a brief overview of some of the more significant findings. We compared the morphology and photocurrent efficiency for films of TH-PPE adsorbed onto single crystal rutile substrates from DMF and MeOH solutions. Figure 26 below compares the AFM images of the films at various deposition times from MeOH (polymer concentration 8.3 μg/mL), and 10 min deposition time from DMF with various polymer concentrations. Interestingly, very different polymer morphology is seen when the CPE is deposited from the two solvents. From DMF at early times, the polymer appears to adsorb as a molecular film, with the images showing what may be individual polymer chains or small aggregates. With increased concentration from DMF, polymer aggregates are present. By contrast, at all times after deposition from MeOH the polymer appears to deposit as aggregates; however, with increased deposition time the polymer aggregates reconstruct on the surface, perhaps as individual chains become adsorbed at the metal oxide surface. Comparison of the optical absorption of the films deposited from the different solvents shows that under the same deposition conditions, films from MeOH give a greater absorption. In accord with this, the IPCE (incident photon to current efficiency) response of the MeOH deposited films is considerably larger. However, after correcting for light absorbed by the films, the APCE (absorbed photon to current efficiency) of the from MeOH is comparable to that from DMF, despite the difference in absolute absorptance of the films.[14]

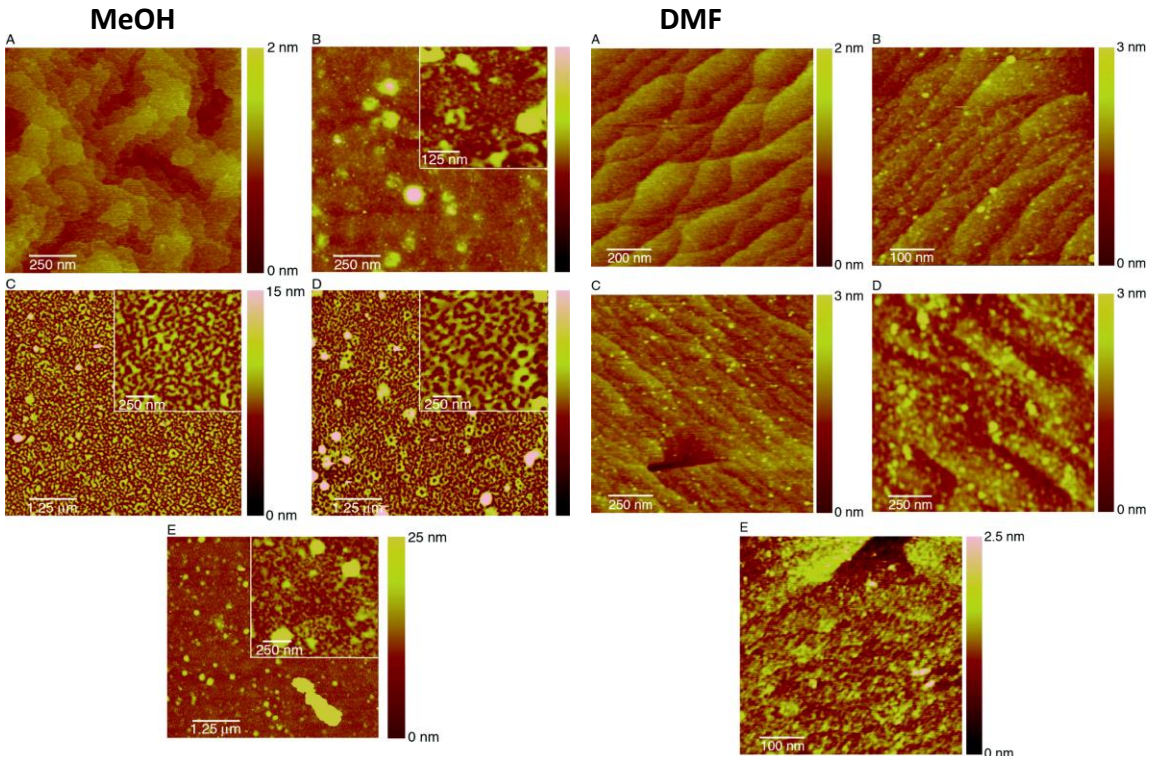

Figure 26. Left set (MeOH) : AFM images of (A) bare rutile (110) and after exposure to a stock solution of 8.3 μg/mL TH in methanol for (B) 15 s, (C) 3 min, (D) 57 min, and (E) 17.5 h. Right set (DMF): AFM images of (A) bare rutile (001) and after a 10 min exposure to (B) 1.6 μg/mL, (C) 3.4 μg/mL, and (D, E) 54.0 μg/mL solutions of TH in DMF.

6.2. Conjugated Polyelectrolytes at Nanostructured TiO_2 Interfaces. Effects of Polymer Chain Length on Light Harvesting Efficiency

In a continuing line of investigation[11,53] we have been exploring the interaction of conjugated polyelectrolytes with nanocrystalline (nc) TiO_2 films films, as well as the ability of these films to undergo photoinduced charge injection and produce photocurrent in a photoelectrochemical cell configuration. In the course of a study on the low bandgap polymer **poly-T$_3$BTD** (see Figure 27), we discovered a remarkable dependence of the adsorption on the polymer chain length (DP = degree of polymerization).[11] In particular, Figure 27a illustrates the absorption of a set of identical TiO_2 films that were exposed to solutions of **poly-T$_3$BTD** for 30 hours. The **poly-T$_3$BTD** samples that were used to prepare the deposition solutions differed in the DP of the polymer; specifically, samples with DP = 5, 8 and 11 were used. The results show that the amount of polymer adsorbed *increases as the DP of the polymer decreases.* The effect of DP on **poly-T$_3$BTD** is mirrored by photocurrent measurements carried out in a photoelectrochemical cell configuration. In particular, as shown in Figure 27b, the IPCE, as determined from the short circuit photocurrent under monochromatic illumination, varies inversely with DP. The maximum peak IPCE of 60% is achieved for the lowest molecular weight sample, and the efficiency drops to 40% for the highest molecular weight sample. Optical absorption study of the films shows that the effects in the IPCE arise due to the difference in absorptance of the films -- in essence the lower DP polymer gives a higher surface coverage and hence harvests a greater fraction of the incident light.

While the effect is completely reproducible, its origin is not fully understood. It is possible that the lower surface coverage for the higher DP polymer arises because the longer chains cannot access the smaller pores within the nanostructured TiO_2. However, it is also possible that the effect arises because the longer chains cannot as easily penetrate into the mesoporous film. These effects will be explored by research outlined in the proposal section.

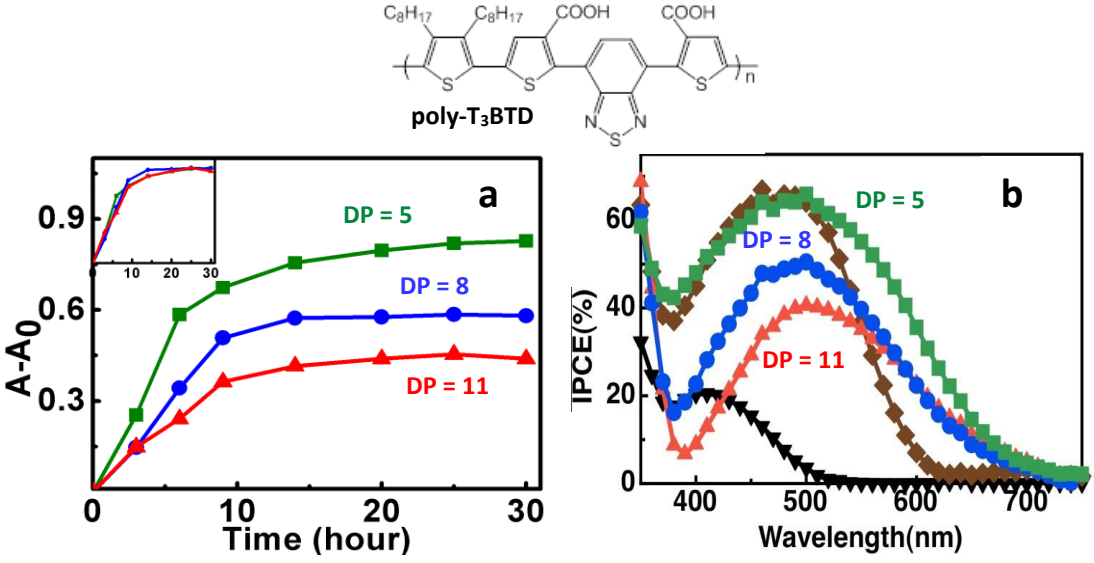

Figure 27. **a**: Time dependent absorption spectrum for adsorption of **poly-T$_3$BTD** onto ns-TiO_2 film from DMF solution. Inset shows the same plots normalized at t = 25 hrs. **b**: Incident photon to current efficiency (IPCE) spectra for **poly-T$_3$BTD**/TiO_2 films in a DSSC photoelectrochemical cell. For each experiment, DP indicates the degree of polymerization for the polymer sample.

6. Summary of Significant Accomplishments

In conclusion, here we highlight the significant accomplishments that have been achieved during the past 30 months in the DOE-BES research program on conjugated polyelectrolytes and donor-acceptor ions:

- Synthesized and characterized the photophysics of the first set of water-soluble, fully conjugated polyelectrolyte dendrimers. Demonstrated that the amplified quenching mechanism operates in the dendrimer structures.
- Investigated the excited state dynamics and the kinetics of energy transfer in ionic and non-ionic conjugated dendrimers. Measured ultrafast dynamics for delocalization of the exciton due to the presence of multiple equivalent chromophores.
- Established that conjugated dendrimers with an energy gradient undergo efficient vectorial energy transfer on timescale of a few ps. Discovered that as the size of the dendrimer increases, the larger number of absorbing units becomes less coupled to the energy acceptor at the core of the dendrimer, lowering the efficiency for energy transfer without changing the time-scale of the process.
- Synthesized and characterized the photophysics of the first set of water soluble, fully conjugated polyelectrolyte oligomers. These oligomers feature fluorescence emission quantum yields approaching unity. Demonstrated amplified quenching effect operates in oligomer systems.
- Studied conjugated polyelectrolytes adsorbed at single crystal TiO_2 interfaces. Show that there is a dependence of morphology on CPE structure and deposition solvent.
- First low band gap conjugated polyelectrolyte deposited at nanostructured-TiO_2 film interface. Discovered an inverse relationship between CPE adsorption and polymer DP. Hybrid CPE-TiO_2 solar cells exhibit very high photocurrent efficiency over a broad wavelength region.
- Developed a family of donor-acceptor-donor compounds containing carboxylate modified benzotriazole (BTz) and benzo(triazole-thiadiazole) (BTzTd) acceptor moieties as light harvesting models for adsorption on oxide semiconductor surfaces. Demonstrated surprisingly poor electron accepting character of the BTz system, while the BTzTd system is strongly accepting.
- Created a new family of fused phenazine based donor-acceptor-donor compounds having controlled conjugation pathways. Demonstrated that the photophysics of these systems are dominated by the substitution pattern at the central acceptor core.

References

1. Skotheim, T. A.; Reynolds, J. R., *Conjugated Polymers: Theory, Synthesis, Properties, and Characterization*; Handbook of Conducting Polymers, 3rd ed.; CRC Press: Boca Raton, FL, 2007; Vol. 1.
2. Skotheim, T. A.; Reynolds, J. R., *Conjugated Polymers: Processing and Applications*; Handbook of Conducting Polymers, 3rd ed.; CRC Press: Boca Raton, FL, 2007; Vol. 2.
3. Cheng, Y. J.; Yang, S. H.; Hsu, C. S., Synthesis of Conjugated Polymers for Organic Solar Cell Applications, *Chem. Rev.* **2009**, *109*, 5868-5923.
4. Clarke, T. M.; Durrant, J. R., Charge Photogeneration in Organic Solar Cells, *Chem. Rev.* **2010**, *110*, 6736-6767.
5. Brabec, C. J.; Gowrisanker, S.; Halls, J. J. M.; Laird, D.; Jia, S. J.; Williams, S. P., Polymer-Fullerene Bulk-Heterojunction Solar Cells, *Adv. Mater.* **2010**, *22*, 3839-3856.
6. Facchetti, A., Pi-Conjugated Polymers for Organic Electronics and Photovoltaic Cell Applications, *Chem. Mater.* **2011**, *23*, 733-758.
7. Pinto, M. R.; Schanze, K. S., Conjugated Polyelectrolytes: Synthesis and Applications, *Synthesis-Stuttgart* **2002**, 1293-1309.
8. Jiang, H.; Taranekar, P.; Reynolds, J. R.; Schanze, K. S., Conjugated Polyelectrolytes: Synthesis, Photophysics, and Applications, *Angew. Chem. Int. Ed.* **2009**, *48*, 4300-4316.
9. Duarte, A.; Pu, K. Y.; Liu, B.; Bazan, G. C., Recent Advances in Conjugated Polyelectrolytes for Emerging Optoelectronic Applications, *Chem. Mater.* **2011**, *23*, 501-515.
10. Lee, S. H.; Kömürlü, S.; Zhao, X. Y.; Jiang, H.; Moriena, G.; Kleiman, V. D.; Schanze, K. S., Water-Soluble Conjugated Polyelectrolytes with Branched Polyionic Side Chains, *Macromolecules* **2011**, *44*, 4742-4751.
11. Fang, Z.; Eshbaugh, A. A.; Schanze, K. S., Low-Bandgap Donor-Acceptor Conjugated Polymer Sensitizers for Dye-Sensitized Solar Cells, *J. Am. Chem. Soc.* **2011**, *133*, 3063-3069.
12. Bricaud, Q.; Fabre, R. M.; Brookins, R. N.; Schanze, K. S.; Reynolds, J. R., Energy Transfer between Conjugated Polyelectrolytes in Layer-by-Layer Assembled Films, *Langmuir* **2011**, *27*, 5021-5028.
13. Komurlu, S.; Lee, S. H.; McCarley, T.; Schanze, K. S.; Kleiman, V. D., Energy Transfer in Extended Thienylene-Phenylene-Ethynylene Dendrimers, *J. Phys. Chem. B* **2011**, *115*, 15214-15220.
14. Sambur, J. B.; Averill, C. M.; Bradley, C.; Schuttlefield, J.; Lee, S. H.; Reynods, J. R.; Schanze, K. S.; Parkinson, B. A., Interfacial Morphology and Photoelectrochemistry of Conjugated Polyelectrolytes Adsorbed on Single Crystal TiO_2, *Langmuir* **2011**, *27*, 11906-11916.
15. Xie, D. P.; Parthasarathy, A.; Schanze, K. S., Aggregation-Induced Amplified Quenching in Conjugated Polyelectrolytes with Interrupted Conjugation, *Langmuir* **2011**, *27*, 11732-11736.
16. Feng, F.; Lee, S. H.; Schanze, K. S., "Light Switch" Effect Upon Binding of Ru-Dppz to Water-Soluble Conjugated Polyelectrolyte Dendrimers, *J. Phys. Chem. Lett.* **2012**, *3*, 1707-1710.

17. Patel, D. G.; Feng, F. D.; Ohnishi, Y. Y.; Abboud, K. A.; Hirata, S.; Schanze, K. S.; Reynolds, J. R., It Takes More Than an Imine: The Role of the Central Atom on the Electron-Accepting Ability of Benzotriazole and Benzothiadiazole Oligomers, *J. Am. Chem. Soc.* **2012**, *134*, 2599-2612.

18. Wu, D.; Feng, F.; Xie, D.; Chen, Y.; Tan, W.; Schanze, K. S., Helical Conjugated Polyelectrolyte Aggregation Induced by Biotin-Avidin Interaction, *J. Phys. Chem. Lett.* **2012**, *3*, 1711-1715.

19. Feng, F.; Lee, S. H.; Cho, S. W.; Kömürlü, S.; McCarley, T.; Roitberg, A.; Kleiman, V. D.; Schanze, K. S., Conjugated Polyelectrolyte Dendrimers: Aggregation, Photophysics and Amplified Quenching, submitted.

20. Vella, J. H.; Bricaud, Q.; Reynolds, J. R.; Schanze, K. S., Aggregation and Singlet Exciton Diffusion in Conjugated Polyelectrolyte Layer-by-Layer Films, submitted.

21. Vella, J. H.; Parthasarathy, A.; Schanze, K. S., Triplet Sensitization in Anionic Conjugated Polyelectrolyte $PPESO_3^-$ by Cationic Ir(III) Complexes, submitted.

22. Lee, S. H.; Kömürlü, S.; McCarley, T. D.; Kleiman, V. D.; Schanze, K. S., Photophysics and Energy Transport in Compact Conjugated Polyelectrolyte Dendrimers, submitted.

23. Kömürlü, S.; Lee, S. H.; Feng, F.; Schanze, K. S.; Kleiman, V. D., Photophysics of Polyelectrolyte and Non-Ionic Phenylene-Ethynylene π-Conjugated Dendrimers, submitted.

24. Kömürlü, S.; Feng, F.; Lee, S. H.; Schanze, K. S.; Kleiman, V. D., Energy Transfer in Conjugated Polyelectrolyte Dendrimers with an Energy Gradient, in preparation.

25. Tan, C.; Atas, E.; Müller, J. G.; Pinto, M. R.; Kleiman, V. D.; Schanze, K. S., Amplified Quenching of a Conjugated Polyelectrolyte by Cyanine Dyes, *J. Am. Chem. Soc.* **2004**, *126*, 13685-13694.

26. Müller, J. G.; Atas, E.; Tan, C.; Schanze, K. S.; Kleiman, V. D., The Role of Exciton Hopping and Direct Energy Transfer in the Efficient Quenching of Conjugated Polyelectrolytes, *J. Am. Chem. Soc.* **2006**, *128*, 4007-4016.

27. Jiang, H.; Zhao, X. Y.; Schanze, K. S., Amplified Fluorescence Quenching of a Conjugated Polyelectrolyte Mediated by Ca^{2+}, *Langmuir* **2006**, *22*, 5541-5543.

28. Jiang, H.; Zhao, X. Y.; Schanze, K. S., Effects of Polymer Aggregation and Quencher Size on Amplified Fluorescence Quenching of Conjugated Polyelectrolytes, *Langmuir* **2007**, *23*, 9481-9486.

29. Zhao, X. Y.; Jiang, H.; Schanze, K. S., Polymer Chain Length Dependence of Amplified Fluorescence Quenching in Conjugated Polyelectrolytes, *Macromolecules* **2008**, *41*, 3422-3428.

30. Lee, S. H.; Feng, F.; Kömürlü, S.; McCarley, T. D.; Kleiman, V. D.; Schanze, K. S., Photophysics of Conjugated Polyelectrolyte Dendrimers with Low Homo-Lumo Gap Core Chromophores, submitted.

31. Chen, L.; McBranch, D. W.; Wang, H.-L.; Helgeson, R.; Wudl, F.; Whitten, D. G., Highly Sensitive Biological and Chemical Sensors Based on Reversible Fluorescence Quenching in a Conjugated Polymer, *Proc. Natl. Acad. Sci. U.S.A.* **1999**, *96*, 12287-12292.

32. Wang, D. L.; Wang, J.; Moses, D.; Bazan, G. C.; Heeger, A. J., Photoluminescence Quenching of Conjugated Macromolecules by Bipyridinium Derivatives in Aqueous Media: Charge Dependence, *Langmuir* **2001**, *17*, 1262-1266.

33. Fan, C.; Hirasa, T.; Plaxco, K. W.; Heeger, A. J., Photoluminescence Quenching of Water-Soluble Conjugated Polymers by Viologen Derivatives: Effect of Hydrophobicity, *Langmuir* **2003**, *19*, 3554-3556.

34. Conjugated Polyelectrolytes Based on Poly(Arylene ethynylene): Synthesis, Solution Photophysics and Applications to Sensors and Solar Cells, Zhao, X., Ph.D. Dissertation, University of Florida, Gainesville, FL, USA, 2007.

35. Tan, C.; Pinto, M. R.; Schanze, K. S., Photophysics, Aggregation and Amplified Quenching of a Water-Soluble Poly(phenylene ethynylene), *Chem. Commun.* **2002**, 446-447.

36. Hall, R. D.; Valeur, B.; Weber, G., Polarization of the Fluorescence of Triphenylene - a Planar Molecule with 3-Fold Symmetry, *Chem. Phys. Lett.* **1985**, *116*, 202-205.

37. Magde, D.; Webb, W. W.; Elson, E., Thermodynamic Fluctuations in a Reacting System - Measurement by Fluorescence Correlation Spectroscopy, *Phys Rev Lett* **1972**, *29*, 705-708.

38. Haustein, E.; Schwille, P., Fluorescence Correlation Spectroscopy: Novel Variations of an Established Technique, *Annu Rev Biophys Biomol Struct* **2007**, *36*, 151-69.

39. Krichevsky, O.; Bonnet, G., Fluorescence Correlation Spectroscopy: The Technique and Its Applications, *Rep. Prog. Phys.* **2002**, *65*, 251-297.

40. Lakowicz, J. R., *Topics in Fluorescence Spectroscopy*, Plenum Press: New York, 1991.

41. Yue, H. J.; Wu, M. Y.; Xue, C. H.; Velayudham, S.; Liu, H. Y.; Waldeck, D. H., Evolution in the Supramolecular Complexes between Poly(phenylene ethynylene)-Based Polyelectrolytes and Octadecyltrimethylammonium Bromide as Revealed by Fluorescence Correlation Spectroscopy, *J. Phys. Chem. B* **2008**, *112*, 8218-8226.

42. Xu, Z. H.; Tsai, H. H.; Wang, H. L.; Cotlet, M., Solvent Polarity Effect on Chain Conformation, Film Morphology, and Optical Properties of a Water-Soluble Conjugated Polymer, *J. Phys. Chem. B* **2010**, *114*, 11746-11752.

43. Chen, C.-Y.; Wang, M.; Li, J.-Y.; Pootrakulchote, N.; Alibabaei, L.; Ngoc-le, C.-h.; Decoppet, J.-D.; Tsai, J.-H.; Grätzel, C.; Wu, C.-G.; Zakeeruddin, S. M.; Grätzel, M., Highly Efficient Light-Harvesting Ruthenium Sensitizer for Thin-Film Dye-Sensitized Solar Cells, *ACS Nano* **2009**, *3*, 3103-3109.

44. Yella, A.; Lee, H. W.; Tsao, H. N.; Yi, C. Y.; Chandiran, A. K.; Nazeeruddin, M. K.; Diau, E. W. G.; Yeh, C. Y.; Zakeeruddin, S. M.; Gratzel, M., Porphyrin-Sensitized Solar Cells with Cobalt (II/III)-Based Redox Electrolyte Exceed 12 Percent Efficiency, *Science* **2011**, *334*, 629-634.

45. Mishra, A.; Fischer, M. K. R.; Bauerle, P., Metal-Free Organic Dyes for Dye-Sensitized Solar Cells: From Structure: Property Relationships to Design Rules, *Angew. Chem.-Int. Edit.* **2009**, *48*, 2474-2499.

46. Hagfeldt, A.; Boschloo, G.; Sun, L. C.; Kloo, L.; Pettersson, H., Dye-Sensitized Solar Cells, *Chem. Rev.* **2010**, *110*, 6595-6663.

47. Balan, A.; Baran, D.; Gunbas, G.; Durmus, A.; Ozyurt, F.; Toppare, L., One Polymer for All: Benzotriazole Containing Donor-Acceptor Type Polymer as a Multi-Purpose Material, *Chem. Commun.* **2009**, 6768-6770.

48. Price, S. C.; Stuart, A. C.; Yang, L. Q.; Zhou, H. X.; You, W., Fluorine Substituted Conjugated Polymer of Medium Band Gap Yields 7% Efficiency in Polymer-Fullerene Solar Cells, *J. Am. Chem. Soc.* **2011**, *133*, 4625-4631.

49. Shirota, Y.; Kageyama, H., Charge Carrier Transporting Molecular Materials and Their Applications in Devices, *Chem. Rev.* **2007**, *107*, 953-1010.

50. Rieger, R.; Beckmann, D.; Mavrinskiy, A.; Kastler, M.; Mullen, K., Backbone Curvature in Polythiophenes, *Chem. Mater.* **2010**, *22*, 5314-5318.

51. Glendening, E. D.; Landis, C. R.; Weinhold, F., Natural Bond Orbital Methods, *Wiley Interdisciplinary Reviews-Computational Molecular Science* **2012**, *2*, 1-42.

52. Spitler, M. T.; Parkinson, B. A., Dye Sensitization of Single Crystal Semiconductor Electrodes, *Acc. Chem. Res.* **2009**, *42*, 2017-2029.

53. Jiang, H.; Zhao, X.; Shelton, A. H.; Lee, S. H.; Reynolds, J. R.; Schanze, K. S., Variable-Band-Gap Poly(Arylene ethynylene) Conjugated Polyelectrolytes Adsorbed on Nanocrystalline TiO_2: Photocurrent Efficiency as a Function of the Band Gap, *ACS Appl. Mater. Interf.* **2009**, *1*, 381.

54. Saji, V. S.; Zong, K.; Pyo, M., Nir-Absorbing Poly(Thieno 3,4-B Thiophene-2-Carboxylic Acid) as a Polymer Dye for Dye-Sensitized Solar Cells, *Journal Of Photochemistry And Photobiology A-Chemistry* **2010**, *212*, 81-87.

55. Bhongale, C. J.; Thelakkat, M., Efficient Hybrid Polymer/Titania Solar Cells Sensitized with Carboxylated Polymer Dye, *Sol. Energy Mater. Sol. Cells* **2010**, *94*, 817-822.

56. Kim, Y. G.; Walker, J.; Samuelson, L. A.; Kumar, J., Efficient Light Harvesting Polymers for Nanocrystalline TiO2 Photovoltaic Cells, *Nano Letters* **2003**, *3*, 523-525.

57. Arango, A. C.; Carter, S. A.; Brock, P. J., Charge Transfer in Photovoltaics Consisting of Interpenetrating Networks of Conjugated Polymer and TiO_2 Nanoparticles, *App. Phys. Lett.* **1999**, *74*, 1698-1700.